

GDF15 links adipose tissue lipolysis with anxiety

Received: 27 August 2024

Accepted: 6 March 2025

Published online: 15 April 2025

 Check for updates

Logan K. Townsend^{1,2}, Dongdong Wang^{1,2}, Carly M. Knuth³, Russta Fayyazi^{1,2}, Ahmad Mohammad⁴, Léa J. Becker⁵, Evangelia E. Tsakiridis^{1,2}, Eric M. Desjardins^{1,2}, Zeel Patel^{1,2}, Celina M. Valvano^{1,2}, Junfeng Lu^{1,2}, Alice E. Payne^{1,2}, Ofure Itua^{1,6}, Kyle D. Medak⁷, Daniel M. Marko^{1,6,8}, Jonathan D. Schertzer^{1,6,8}, David C. Wright^{9,10,11}, Shawn M. Beaudette¹², Katherine M. Morrison^{1,13}, André C. Carpentier¹⁴, Denis P. Blondin¹⁴, Rebecca E. K. MacPherson¹⁴, Jordan G. McCall⁵, Marc G. Jeschke^{15,16,17} & Gregory R. Steinberg^{1,2,6} ✉

Psychological stress changes both behaviour and metabolism to protect organisms. Adrenaline is an important driver of this response. Anxiety correlates with circulating free fatty acid levels and can be alleviated by a peripherally restricted β -blocker, suggesting a peripheral signal linking metabolism with behaviour. Here we show that adrenaline, the β_3 agonist CL316,243 and acute restraint stress induce growth differentiation factor 15 (GDF15) secretion in white adipose tissue of mice. Genetic inhibition of adipose triglyceride lipase or genetic deletion of β -adrenergic receptors blocks β -adrenergic-induced increases in GDF15. Increases in circulating GDF15 require lipolysis-induced free fatty acid stimulation of M2-like macrophages within white adipose tissue. Anxiety-like behaviour elicited by adrenaline or restraint stress is eliminated in mice lacking the GDF15 receptor GFRAL. These data provide molecular insights into the mechanisms linking metabolism and behaviour and suggest that inhibition of GDF15–GFRAL signalling might reduce acute anxiety.

The incidence of anxiety disorders has rapidly increased over the last two decades, and anxiety is now the most prevalent psychiatric disorder, affecting nearly 30% of the Western population at some point¹. Acute stress-induced anxiety helps maintain the arousal and vigilance required to avoid repeated exposures to dangerous conditions^{2,3}. Catecholamines, namely noradrenaline and adrenaline (international nonproprietary names: norepinephrine and epinephrine, respectively), are critical to coordinating the central and peripheral responses to psychological stress^{3–6}.

Central noradrenaline, particularly from the locus coeruleus, is known to control acute anxiety-like behaviour^{3,4}. Interestingly, acute peripheral administration of adrenaline also produces anxiety^{5–9}, despite adrenaline not crossing the blood–brain barrier, and this effect is abolished by the β -blocker propranolol^{10–13}. Central mechanisms could explain the effects of propranolol, which readily crosses the

blood–brain barrier; however, treatment with practolol, a β -blocker that does not cross the blood–brain barrier, elicits similar anxiolytic effects¹⁴. These studies suggest that there may be peripheral endocrine signals linking β -adrenergic signalling with behaviour that have yet to be identified.

Growth differentiation factor 15 (GDF15) is a distant member of the transforming growth factor- β superfamily that circulates at low levels under normal physiological conditions but is elevated during cellular stress and mitochondrial diseases^{15,16}. GDF15 signals through its receptor, glial-cell-derived neurotrophic factor receptor α -like (GFRAL), which is found exclusively in the brainstem¹⁷. GDF15–GFRAL signalling leads to behavioural changes, including reduced food intake¹⁸, nausea¹⁹ and aversive^{19,20} and anxiety-like behaviours^{20–22}. These effects may involve activation of the sympathetic and hypothalamic–pituitary–adrenal (HPA) axes^{23–26}, both of which are classic responses to

A full list of affiliations appears at the end of the paper. ✉ e-mail: gstein@mcmaster.ca

psychological stress. In this study, we aimed to identify potential links between peripheral β -adrenergic activity and anxiety. We show that β -adrenergic stimulation activates adipocyte lipolysis, which promotes the secretion of GDF15 from adipose tissue-resident macrophages, ultimately linking changes in peripheral metabolism with behaviour.

Results

Psychological stress increases GDF15 through β -adrenergic signalling

Adipose tissue is a major endocrine organ that links metabolism with neuronal circuits and is acutely sensitive to changes in β -adrenergic signalling^{5–10,13,27}. We treated mice with saline or adrenaline injected intraperitoneally (IP) (Fig. 1a). In agreement with previous studies²⁸, adrenaline induced anxiety-like behaviour without affecting overall activity levels (Fig. 1b). To identify adipose-derived endocrine signals, we collected gonadal white adipose tissue (gWAT) and serum 1 h after treatment with saline or the same dose of adrenaline from another cohort of mice. As anticipated²⁹, adrenaline produced marked and distinct separation in principal component analysis (Fig. 1c), with the most upregulated differentially expressed genes (DEGs) associated with the unfolded protein response and thermogenic and adaptive gene signatures (Fig. 1d and Extended Data Fig. 1a). From this gene set, we then isolated genes encoding secreted protein products (that is, ligands)³⁰ and found that *Gdf15* was the most highly upregulated ($P = 6.59 \times 10^{-29}$) secreted factor, showing a >4 log₂-fold increase in adrenaline-treated mice compared with saline-treated mice (Fig. 1e and Extended Data Fig. 1b); indeed, *Gdf15* was one of the most upregulated genes in gWAT. Corresponding with elevations in gWAT *Gdf15* mRNA, GDF15 protein in serum was increased nearly five-fold within 1 h and remained elevated up to 4 h after injection (Fig. 1f). Reverse transcription followed by qPCR confirmed that adrenaline produced an approximately eight-fold increase in *Gdf15* in gWAT without affecting *Gdf15* in the liver, kidney, subcutaneous inguinal WAT (iWAT) or brown adipose tissue (Fig. 1g). *Gdf15* expression was slightly increased in the lung and heart but was undetectable in skeletal muscle (Fig. 1g). Consistent with lower gWAT mass, serum GDF15 levels were lower in age-matched female mice than in male mice, but the relative response to adrenaline was similar between sexes (Extended Data Fig. 1c). Adrenaline also induced a similar increase in GDF15 whether mice were housed at room temperature or thermoneutrality (Extended Data Fig. 1d). These data indicate that adrenaline leads to marked increases in gWAT and serum GDF15 in mice.

Previous studies characterizing GDF15-null mice found that these animals exhibit less anxiety-like behaviour in open-field and elevated-plus tests^{21,22}. Psychological stress can be acutely induced in mice by changing their cages, whereas chronic single housing for 3 days is a form of long-term psychological stress³¹. We found that, consistent with adrenaline injection, acute cage change increased serum GDF15 levels; however, single housing did not (Fig. 1h). Consistent with our observations in mice that chronic stress and GDF15 are not linked, two-sample Mendelian randomization (2SMR) of GDF15 within the UK Biobank and serum GDF15 in children who were overweight and obese did not show associations with anxiety (Extended Data Fig. 2a–c). Although coding polymorphisms affect the measurement of circulating GDF15 in humans³², these data suggest that adrenergic-induced GDF15 may be involved in acute but not chronic psychological stress.

An acute psychological stress that reliably increases adrenaline in mice is physical restraint³³. We observed increased circulating adrenaline following acute physical restraint, although the levels were lower than after treatment with IP injected adrenaline (Extended Data Fig. 1e). Adrenaline signals in adipose tissue through β -adrenergic receptors³⁴. Therefore, to examine whether psychological stress induces GDF15 through β -adrenergic receptors, we physically restrained wild-type (WT) mice and mice lacking β_1 , β_2 and β_3 adrenergic receptors (*Adrb1*, *Adrb2* and *Adrb3* triple knockout (BR^{-/-})) in 50-ml conical tubes (Fig. 1i).

Restraint of WT mice increased serum and gWAT GDF15; however, this response was eliminated in BR^{-/-} mice (Fig. 1j,k). Baseline GDF15 levels were indistinguishable between genotypes and, importantly, lipopolysaccharide (LPS) increased serum GDF15 levels³⁵ and lowered blood glucose levels similarly in WT and BR^{-/-} mice (Extended Data Fig. 3a,b), demonstrating that these mice have an intact GDF15 response to non- β -adrenergic stimuli. These results show that psychological stress increases GDF15 and that this is dependent on β -adrenergic signalling.

ATGL is critical for promoting β -adrenergic-induced GDF15

Lipolysis is a major regulator of the transcriptional responses within adipose tissue²⁹ and is increased by β -adrenergic-induced activation of adipose triglyceride lipase (ATGL), the rate-limiting enzyme for the release of free fatty acids from WAT³⁶. To determine whether ATGL is responsible for regulating GDF15 secretion from adipose tissue, we treated adipocyte-specific ATGL-knockout mice (AdATGL^{-/-}) and their floxed littermate controls (AdATGL^{lox/lox}) with IP injected saline or CL316,243 (CL), a potent and selective β_3 -adrenergic agonist. ATGL expression was ~90% lower in gWAT of AdATGL^{-/-} mice (Fig. 2a). CL increased serum nonesterified fatty acids and markers of the unfolded protein response, *Atf4* and *Chop*, in gWAT of AdATGL^{lox/lox} animals (Fig. 2b–d). These responses were eliminated in AdATGL^{-/-} mice despite β -adrenergic signalling remaining intact, as evidenced by the similar increase in *Ppargc1a* expression and phosphorylation of cAMP-dependent protein kinase (PKA) substrates in AdATGL^{-/-} and floxed mice (Fig. 2e,f). Consistent with our observations in BR^{-/-} mice, basal GDF15 levels were similar between AdATGL^{lox/lox} and AdATGL^{-/-} mice; however, CL-induced increases in circulating and gWAT GDF15 were eliminated in AdATGL^{-/-} mice (Fig. 2g,h). Treatment with IP injected cilostamide, a phosphodiesterase-3 inhibitor that leads to increased cellular cAMP levels, exaggerated the effects of CL on circulating GDF15 levels (Fig. 2i), supporting the involvement of the β_3 adrenergic receptor–cAMP–ATGL pathway in stimulating GDF15.

Physical restraint stress promotes adipose tissue lipolysis³⁷. Serum glycerol was increased in AdATGL^{lox/lox} but not in AdATGL^{-/-} mice in response to acute tube restraint (Fig. 2j). Similarly, circulating GDF15 levels were increased in AdATGL^{lox/lox} but not in AdATGL^{-/-} mice (Fig. 2k). We tested the behavioural response to acute restraint stress in these mice, but AdATGL^{-/-} mice became hypoglycaemic following restraint, and this was associated with marked reductions in overall activity during open-field tests (Extended Data Fig. 4a–c), an effect that was likely secondary to the defect in adipose tissue lipolysis.

To evaluate whether β -adrenergic signalling increases GDF15 in a cell-autonomous manner, we cultured and differentiated mouse white adipocytes before treating them with CL and the ATGL inhibitor ATGListatin³⁸. As expected, CL increased glycerol release in the medium, and this was blocked by ATGListatin; however, neither CL nor ATGListatin altered GDF15 levels in the medium (Fig. 2l,m). These data suggest that GDF15 is unlikely to be derived from adipocytes in response to adrenergic stimulation.

As adipocyte-specific ablation of ATGL inhibited GDF15 secretion but isolated adipocytes did not secrete GDF15 in response to CL, we hypothesized that another cell type within adipose tissue might be responsible for GDF15 secretion. To test this, we fractionated gWAT and iWAT into adipocytes and the stromal vascular fraction (SVF). Consistent with our hypothesis and recent studies³⁹, *Gdf15* expression was higher in the SVF of both WAT depots but particularly in gWAT (Fig. 2n). Moreover, in response to IP injected adrenaline, *Gdf15* was increased in only the SVF (Fig. 2o), whereas the related cytokine, *Fgf21*, was increased in only the adipocyte fraction (Extended Data Fig. 5a). Appropriate separation was confirmed as leptin was found only in the adipocyte fraction (Extended Data Fig. 5b). These results point towards ATGL-dependent intercellular communication mediating β -adrenergic-induced adipose tissue GDF15 secretion.

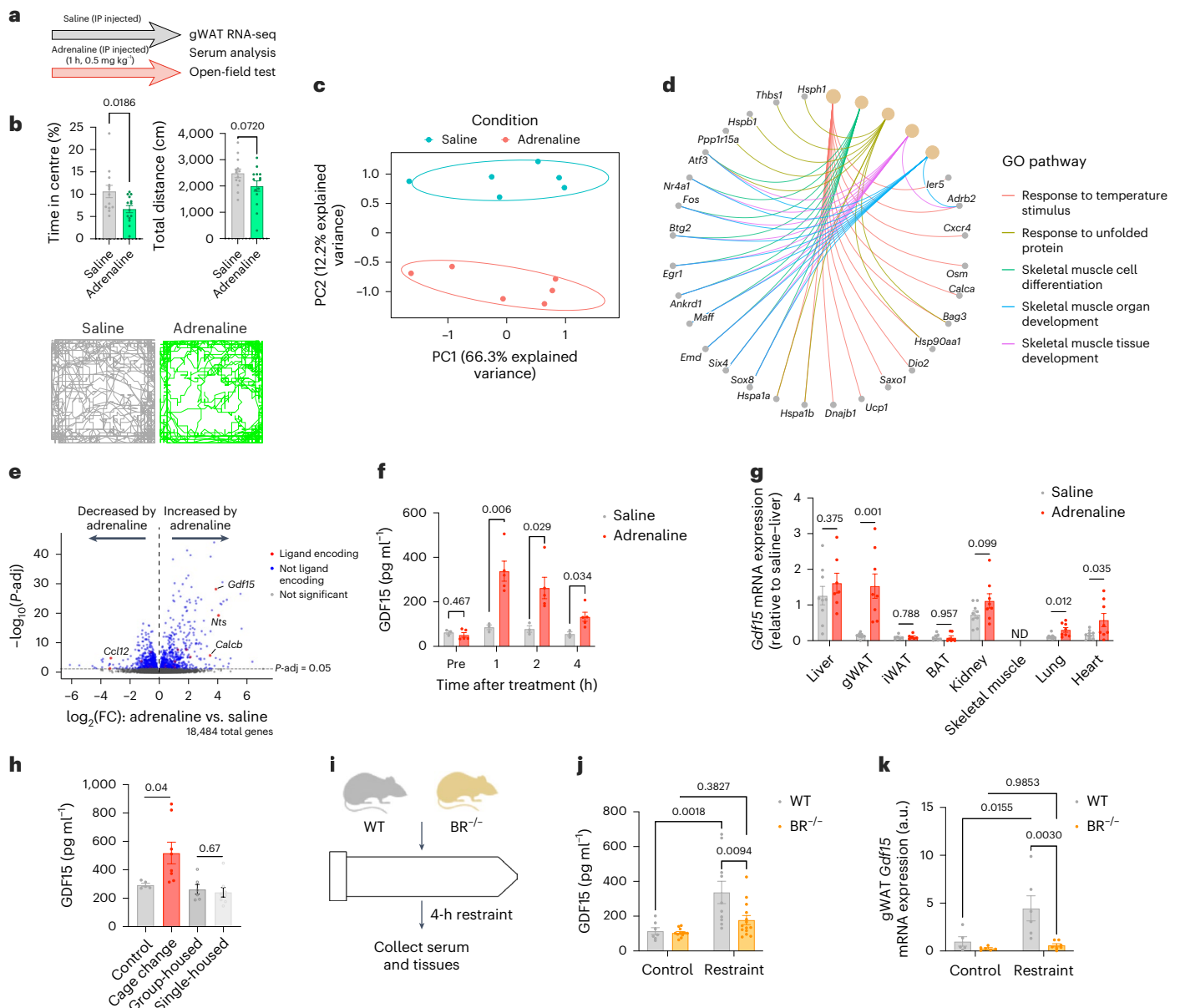


Fig. 1 | Acute psychological stress and adrenergic signalling increase GDF15 levels from gWAT. **a**, Schematic of acute vehicle and adrenaline treatment and analyses. **b**, Top: time in the centre and total distance travelled during an open-field test 1 h following treatment with adrenaline (*n* = 14) or saline (*n* = 13). Bottom: representative images of movements of individual mice. Data are presented as mean ± s.e.m. with *P* values calculated using an unpaired two-tailed *t* test. **c**, Principal component analysis of gWAT samples from saline-treated (*n* = 6) and adrenaline-treated (*n* = 6) mice using VST data from DESeq2. **d**, Gene-concept network diagram indicating the corresponding enriched Gene Ontology (GO) terms according to DEGs between saline-treated (*n* = 6) and adrenaline-treated (*n* = 6) gWAT. **e**, Volcano plot showing DEGs identified between saline- and adrenaline-treated gWAT. The *P*-adj was calculated using the Benjamini–Hochberg method. FC, fold change. **f**, Time course of circulating GDF15 before and after adrenaline (*n* = 5) or saline (*n* = 3) treatment. Data are presented as mean ± s.e.m. with *P* values calculated using an unpaired two-tailed *t* test. **g**, Tissue screen of *Gdf15* in mice 1 h after adrenaline (*n* = 8) or

saline (*n* = 9) treatment. Data are expressed relative to the saline-treated liver. Data are presented as mean ± s.e.m. with *P* values calculated using an unpaired two-tailed *t* test. ND, not detected; BAT, brown adipose tissue. **h**, Serum GDF15 levels in mice from the following groups: maintained in their home cage (*n* = 5), with cage change for 30 min (*n* = 8), group-housed (*n* = 6) or single-housed for 3 days (*n* = 8). Data are presented as mean ± s.e.m. with *P* values calculated using an unpaired two-tailed *t* test. **i**, Schematic of an acute restraint test in WT and *Adrb1*, *Adrb2* and *Adrb3* triple knockout (BR^{-/-}) mice. **j**, Serum GDF15 levels in WT and BR^{-/-} mice following 4 h of tube restraint (WT *n* = 10, BR^{-/-} *n* = 14) or the control condition (WT *n* = 9, BR^{-/-} *n* = 12). Data are presented as mean ± s.e.m. with *P* values calculated using a two-way ANOVA with post hoc testing and Tukey's correction. **k**, gWAT *Gdf15* expression levels in WT and BR^{-/-} mice following 4 h of tube restraint (WT *n* = 6, BR^{-/-} *n* = 7) or the control condition (WT *n* = 5, BR^{-/-} *n* = 6). a.u., arbitrary units. Data are presented as mean ± s.e.m. with *P* values calculated using a two-way ANOVA with post hoc testing and Tukey's correction.

Macrophages are the primary source of serum GDF15

To determine the probable cell type secreting GDF15 in adipose tissue, we analysed publicly available single-cell RNA-sequencing (scRNA-seq) data of cells from gWAT of CL-treated mice⁴⁰. Cells were divided into either lineage marker positive (Lin⁺) (including monocytes,

macrophages and B cells) or Lin⁻ (including fibroblasts and adipocytes). *Gdf15* was primarily expressed in Lin⁺ cell types, especially in macrophages (Fig. 3a,b), with negligible expression in any Lin⁻ cell type, including adipocytes (Extended Data Fig. 5c). In response to CL treatment, there was increased *Gdf15* expression only in the macrophage

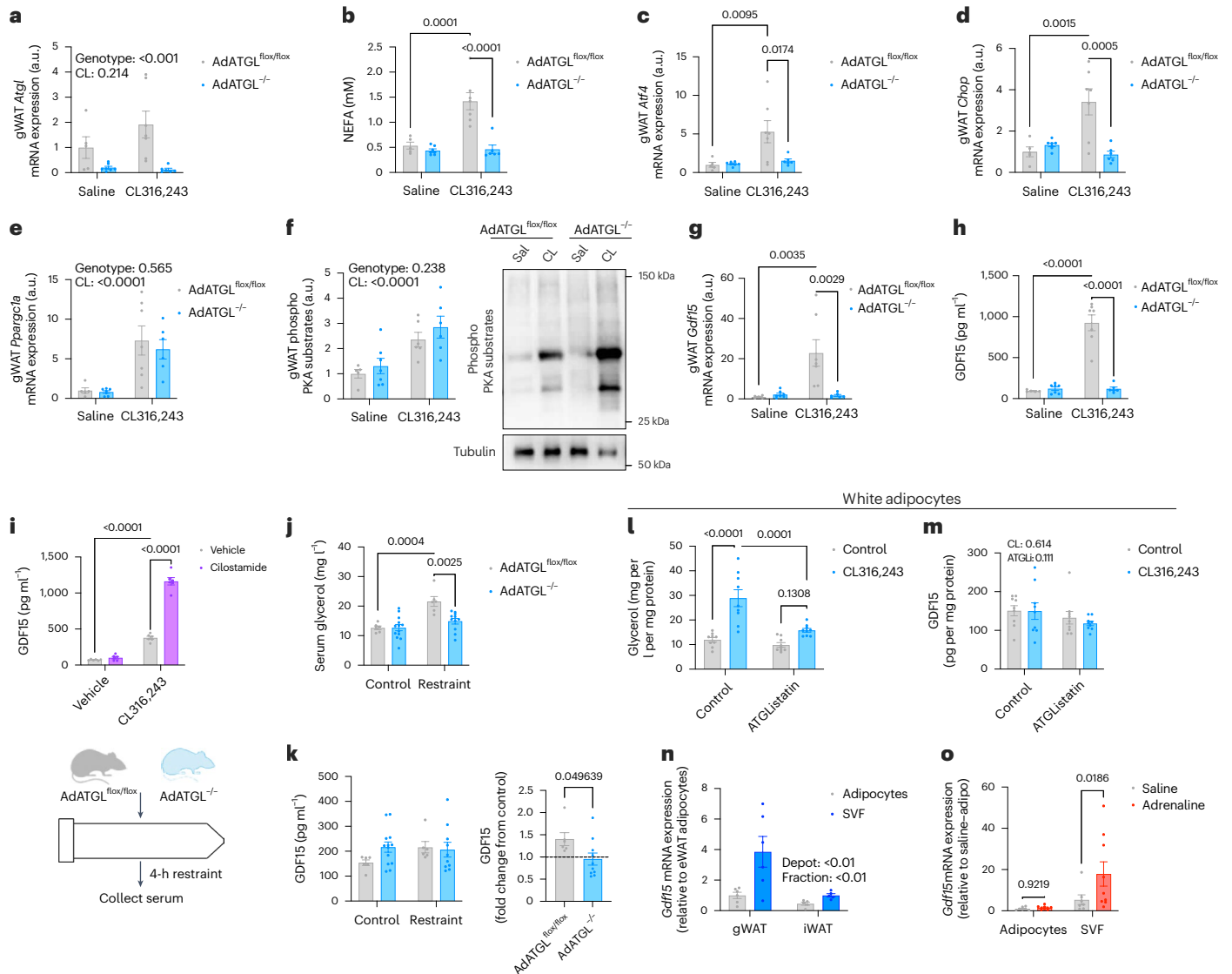


Fig. 2 | Adipocyte ATGL is critical for adrenergic-induced GDF15 secretion from the SVF. **a–g**, gWAT *Atgl* expression (**a**), serum nonesterified fatty acids (NEFA) (**b**), gWAT *Atf4* expression (**c**), gWAT *Chop* expression (**d**), gWAT *Ppargc1a* expression (**e**), gWAT phosphorylated PKA substrates with a representative Western blot image (**f**) and gWAT *Gdf15* expression in AdATGL^{flox/flox} (saline $n = 5$, CL $n = 7$) and AdATGL^{-/-} (saline $n = 7$, CL $n = 6$) mice (**g**). Data are presented as mean \pm s.e.m. with P values calculated using a two-way ANOVA with post hoc testing and Tukey's correction. **h**, Circulating GDF15 levels in AdATGL^{flox/flox} (saline $n = 5$, CL $n = 7$) and AdATGL^{-/-} (saline $n = 7$, CL $n = 6$) mice. Data are presented as mean \pm s.e.m. with P values calculated using a two-way ANOVA with post hoc testing and Tukey's correction. **i**, Top: serum GDF15 after 1 h of CL and cilostamide cotreatment in mice ($n = 6$ per group). Data are presented as mean \pm s.e.m. with P values calculated using a two-way ANOVA with post hoc testing and Tukey's correction. Bottom: schematic of the acute restraint test in AdATGL^{flox/flox} and AdATGL^{-/-} mice. **j**, Serum glycerol levels in AdATGL^{flox/flox} mice (control $n = 6$, restraint $n = 6$) and AdATGL^{-/-} mice (control $n = 13$, restraint $n = 11$) following restraint. Data are presented as mean \pm s.e.m. with P values calculated using a

two-way ANOVA with post hoc testing and Tukey's correction. **k**, Left: serum GDF15 in AdATGL^{flox/flox} mice (control $n = 6$, restraint $n = 6$) and AdATGL^{-/-} mice (control $n = 13$, restraint $n = 11$). Right: graph showing the fold change. Data are presented as mean \pm s.e.m. with P values calculated using a two-way ANOVA (left) and an unpaired two-tailed t test (right). **l**, Glycerol levels in medium from white adipocytes treated with CL and/or ATGListatin ($n = 9$ per group; individual data points from three independent experiments). Data are presented as mean \pm s.e.m. with P values calculated using a two-way ANOVA with post hoc testing and Tukey's correction. **m**, GDF15 levels in medium from white adipocytes treated with CL and/or ATGListatin ($n = 9$ per group; individual data points from three independent experiments). Data are presented as mean \pm s.e.m. with P values calculated using a two-way ANOVA with post hoc testing and Tukey's correction. **n**, *Gdf15* expression in adipocytes and SVF from gWAT ($n = 6$) and iWAT ($n = 5$) of mice. Data are presented as mean \pm s.e.m. with P values calculated using a two-way ANOVA. **o**, *Gdf15* expression in adipocytes and SVF from gWAT 1 h after saline ($n = 7$) or adrenaline ($n = 9$) treatment. Data are presented as mean \pm s.e.m. with P values calculated using a two-way ANOVA with post hoc testing and Tukey's correction.

population (Fig. 3a). Because macrophage populations in adipose tissue are highly heterogeneous⁴¹, we used established gene signatures to identify three major clusters of macrophage populations: classically activated M1-like (*Adgre1/F480* and *iNos/Cd86/Cd80*), alternatively activated M2-like (*Adgre1/F480* and *Cd163/Arg1*) and macrophages that express *Adgre1/F480* but no other markers for M1- or M2-like activation (Fig. 3c). We observed that CL led to the accumulation of both M1- and M2-like macrophages in gWAT, as noted in

the original report⁴⁰. CL increased *Gdf15* in M2-like *Adgre1/F480*- and *Cd163/Arg1*-positive macrophages to a greater degree than observed in M1-like macrophages (Fig. 3c,d). We subsequently examined whether increases in *Gdf15* also occurred after acute treatment with adrenaline by isolating F4/80⁺ cells from the SVF of gWAT (Extended Data Fig. 5d). Consistent with the scRNA-seq results, we found that *Gdf15* expression was higher in F4/80⁺ cells than in other cells within the SVF and that adrenaline induced increases in *Gdf15* in F4/80⁺ cells without any

change in F4/80⁺ cells of the SVF (Fig. 3e). Taken together, these data demonstrate that macrophages are the primary source of GDF15 in response to β -adrenergic-induced lipolysis.

Fatty acids are the primary mediators of the transcriptional response to adipocyte lipolysis²⁹. To determine whether fatty acids are responsible for GDF15 secretion from macrophages, we turned to bone marrow-derived macrophages (BMDMs) polarized with LPS + interferon- γ (IFN γ) (M1-like activation) or interleukin-4 (IL-4) (M2-like) or left untreated (M0) (Fig. 3f)⁴². We then treated BMDMs with two of the most abundant fatty acid species that are increased in the circulation by β -adrenergic agonists⁴³, namely oleate, an unsaturated fatty acid, and palmitate, a saturated fatty acid. We also included tunicamycin, a compound that activates the unfolded protein response and is known to increase GDF15 (refs. 44,45). In line with our scRNA-seq results, palmitate and tunicamycin stimulated the secretion of GDF15 only in M0 and M2-like macrophages but not in M1-like macrophages (Fig. 3g). Similar results were seen at the transcriptional level, with *Gdf15* expression being increased by palmitate only in M0 and M2-like macrophages (Fig. 3h). These results align with earlier work showing that adipocytes preferentially secrete palmitate, which is a critical regulator of macrophage metabolism⁴⁶. Macrophage polarization was confirmed by the expression levels of *Arg1* and *iNos*, which were elevated in M2- and M1-like macrophages, respectively (Extended Data Fig. 5e). Under basal conditions, GDF15 secretion into the medium was similar between M1-like and M2-like polarized cells, both of which showed greater GDF15 levels than unpolarized M0 cells (Extended Data Fig. 5f). Importantly, treatment of macrophages with adrenaline did not affect GDF15 secretion (Extended Data Fig. 5g), indicating that adrenergic signalling does not directly stimulate macrophage GDF15 secretion.

We then used these scRNA-seq data to compare the M1- and M2-like macrophage populations to identify possible mechanisms behind the M2-like-specific palmitate-induced GDF15 secretion. M2-like macrophages are known to use fatty acid metabolism to a greater degree than M1-like macrophages; consistent with this, our analysis of the scRNA-seq data found that fatty acid metabolic processes (Fig. 3i) and fatty acid transporters (Extended Data Fig. 5h) were upregulated in M2- compared with M1-like macrophages. Many fatty acid transporters are upregulated by the transcription factor peroxisome proliferator-activated receptor- γ (PPAR γ), which is enriched in M2-like macrophages⁴¹ and was recently shown to increase the secretion of GDF15 from hepatocytes when activated⁴⁷. To determine whether PPAR γ is involved in controlling the secretion of GDF15, we treated M2-like BMDMs with rosiglitazone, a PPAR γ agonist, and T0070907, a PPAR γ antagonist. We observed that rosiglitazone increased GDF15 levels in the medium and that this effect was blocked by T0070907

(Fig. 3j). T0070907 also blocked palmitate-induced GDF15 secretion from M2-like macrophages (Fig. 3k). Together, these data show that palmitate drives the secretion of GDF15 specifically from macrophages polarized to an alternative M2-like phenotype through a mechanism that probably involves PPAR γ .

Feeding mice a diet high in saturated fatty acids can promote anxiety-like behaviour (reviewed in ref. 48). Exogenous delivery of fatty acids such as palm oil by acute oral gavage increases the expression of GDF15 in the kidney and other tissues, and this leads to elevations in serum GDF15, an effect that peaks after 4 h (ref. 49). We tested whether an oral gavage of palm oil can produce anxiety-like behaviour after 4 h and, if so, whether this effect is blunted in mice lacking the receptor for GDF15, GFRAL (*Gfral*^{-/-} mice). In contrast to adrenaline injection or tube restraint, treatment with palm oil did not increase anxiety-like behaviour in either genotype (Extended Data Fig. 6a). We next tested the effects of a high-fat diet predominantly composed of palm oil for 4 weeks and found similarly increased anxiety-like behaviour in both WT and *Gfral*^{-/-} mice (Extended Data Fig. 6b,c). These results suggest that GDF15–GFRAL signalling is not involved in mediating anxiety-like behaviour in response to acute or chronic exogenous fatty acids.

GDF15 promotes anxiety-like behaviour through GFRAL

GDF15 regulates food intake and energy expenditure through its receptor, GFRAL^{15,18,26}, the expression of which is isolated to the area postrema and nucleus tractus solitarius of the hindbrain¹⁷. To date, no other ligands besides GDF15 have been shown to signal through GFRAL. To establish whether GFRAL signalling is important for mediating anxiety-like behaviour, we treated WT or GFRAL-knockout (*Gfral*^{-/-}) mice with IP injected adrenaline (as in Fig. 1a) 1 h before open-field tests. Adrenaline again induced anxiety-like behaviour in WT mice, but this response was lost in *Gfral*^{-/-} mice (Fig. 4a) without affecting total activity (Fig. 4b). Anxiety is also reflected by nonambulatory movements, such as grooming⁵⁰. Further supporting that GFRAL is necessary for the behavioural responses to acute stress, nonambulatory movements were increased in WT but not in *Gfral*^{-/-} mice in response to IP injected adrenaline (Extended Data Fig. 7a); again, total physical activity was not altered by adrenaline (Extended Data Fig. 7b). Other responses to adrenaline, including food intake, energy expenditure and substrate use, were similar between genotypes (Extended Data Fig. 7c–e).

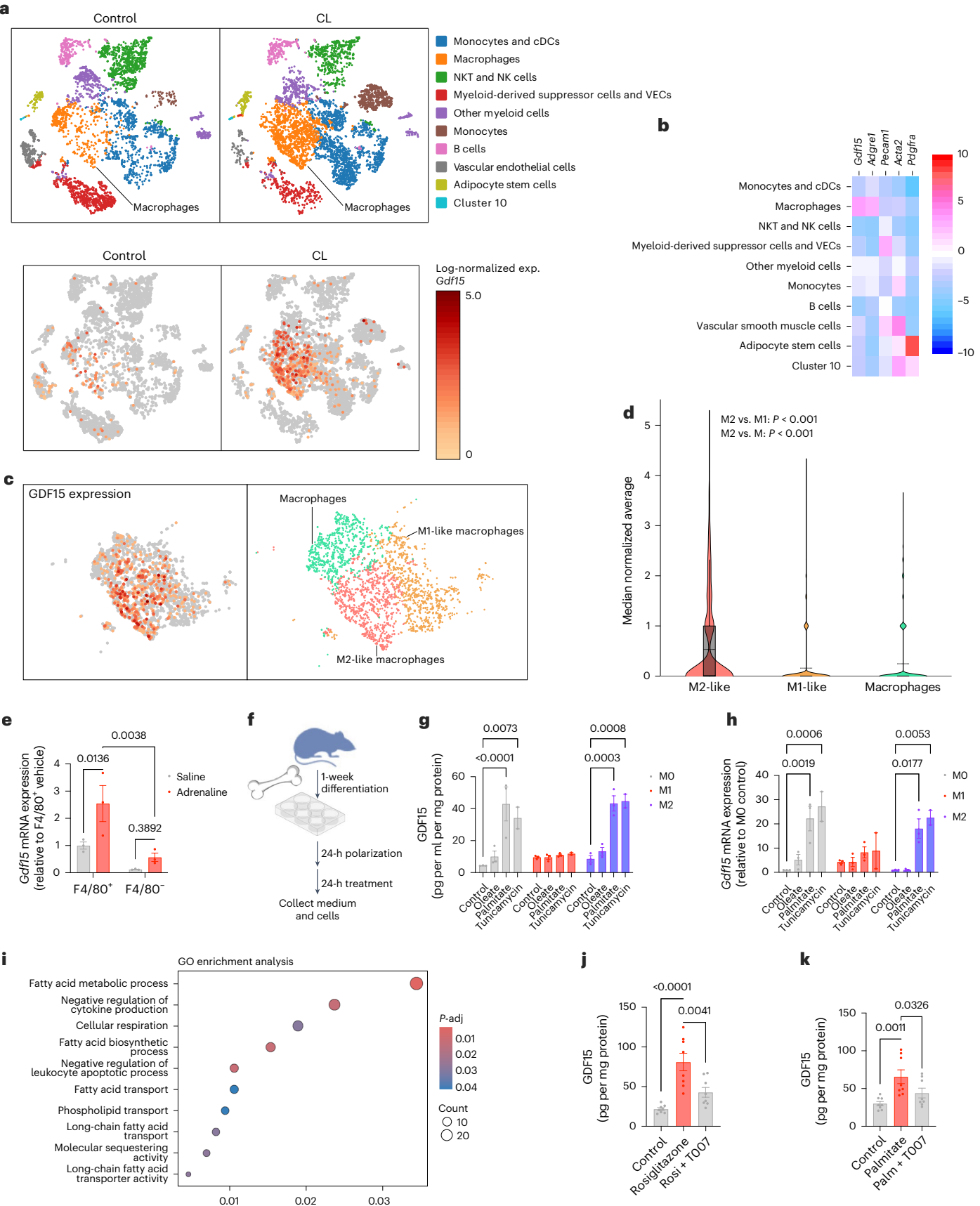
We next tested whether GFRAL is important for the behavioural responses to psychological stress by applying acute physical restraint before the open-field test. As expected³, restraint stress reduced the time spent in the centre, but, remarkably, this response was lost in *Gfral*^{-/-} mice (Fig. 4c). Importantly, this effect was independent of genotypic differences in the total activity levels during the open-field test, which

Fig. 3 | Adipocyte lipolysis mediates GDF15 secretion from alternatively activated M2-like macrophages through fatty acids. **a**, Top: *t*-distributed stochastic neighbour embedding plot of stromal vascular cells from gWAT of mice treated with CL for 3 days. Clustering identified ten major cell types or states. cDCs, conventional dendritic cells; NKT, natural killer T; NK, natural killer; VECs, vascular endothelial cells. Bottom: data were queried for cell clusters expressing *Gdf15*. exp., expression. **b**, Heat map showing the expression of *Gdf15* and other cell-identifying factors in the various cell populations identified in scRNA-seq data. **c**, Data were queried to determine *Gdf15* expression in the identified macrophage populations. **d**, Median normalized average *Gdf15* expression in the M2-like, M1-like and macrophage populations from CL-treated mouse scRNA-seq data. The box-and-whisker plot is defined by the median (centre line) with the first quartile (Q1, lower line), third quartile (Q3, upper line), maximum (Q1 + 1.5 \times interquartile range) and minimum (Q3 + 1.5 \times interquartile range). Whiskers: 1.5 \times (Q3 – Q1). *P* values were calculated using a one-way ANOVA with Benjamini–Hochberg correction for multiple tests. **e**, *Gdf15* expression in mouse F4/80⁺ and F4/80⁻ fractions (*n* = 3 per group). Data are presented as mean \pm s.e.m. with *P* values calculated using a two-way ANOVA with post hoc testing and Tukey's correction. **f**, Experimental schematic of the isolation,

activation and treatment of BMDMs. **g**, GDF15 levels in medium from BMDMs treated with fatty acids (*n* = 3) or tunicamycin (*n* = 2). Individual data points represent triplicates from three independent experiments. Data are presented as mean \pm s.e.m. with *P* values calculated using a two-way ANOVA with post hoc testing and Tukey's correction. **h**, *Gdf15* expression in BMDMs treated with fatty acids (*n* = 3) or tunicamycin (*n* = 2). Data points represent triplicates from three independent experiments. Data are presented as mean \pm s.e.m. with *P* values calculated using a two-way ANOVA with post hoc testing and Tukey's correction. **i**, GO enrichment analysis of M1- and M2-like macrophage populations from scRNA-seq data. The *P*-adj was calculated using the Benjamini–Hochberg method. **j**, GDF15 levels in medium from M2-like BMDMs treated with rosiglitazone (Rosi) or T0070907 (T007) (*n* = 9 per group). Individual data points represent triplicates from three independent experiments. Data are presented as mean \pm s.e.m. with *P* values calculated using a one-way ANOVA with post hoc testing and Tukey's correction. **k**, GDF15 levels in medium from M2-like BMDMs treated with palmitate (Palm) or T0070907 (T007) (*n* = 9 per group). Individual data points represent triplicates from three independent experiments. Data are presented as mean \pm s.e.m. with *P* values calculated using a one-way ANOVA with post hoc testing and Tukey's correction. **l** created using BioRender.com.

were similarly reduced regardless of genotype (Fig. 4d). Anxiety-like behaviour was distinct from food intake or nausea, both of which are altered by stress and can be controlled by GDF15 (ref. 19), given that the same restraint protocol did not affect chow or kaolin clay consumption in

WT or *Gfral*^{-/-} mice (Extended Data Fig. 7f,g); stress-induced hypophagia and nausea have both been attributed to glucagon-like peptide 1 (refs. 51–53). In support of the angiogenic effects of GDF15, a single intraperitoneal injection of a pharmacological dose of GDF15 (ref. 26) produced



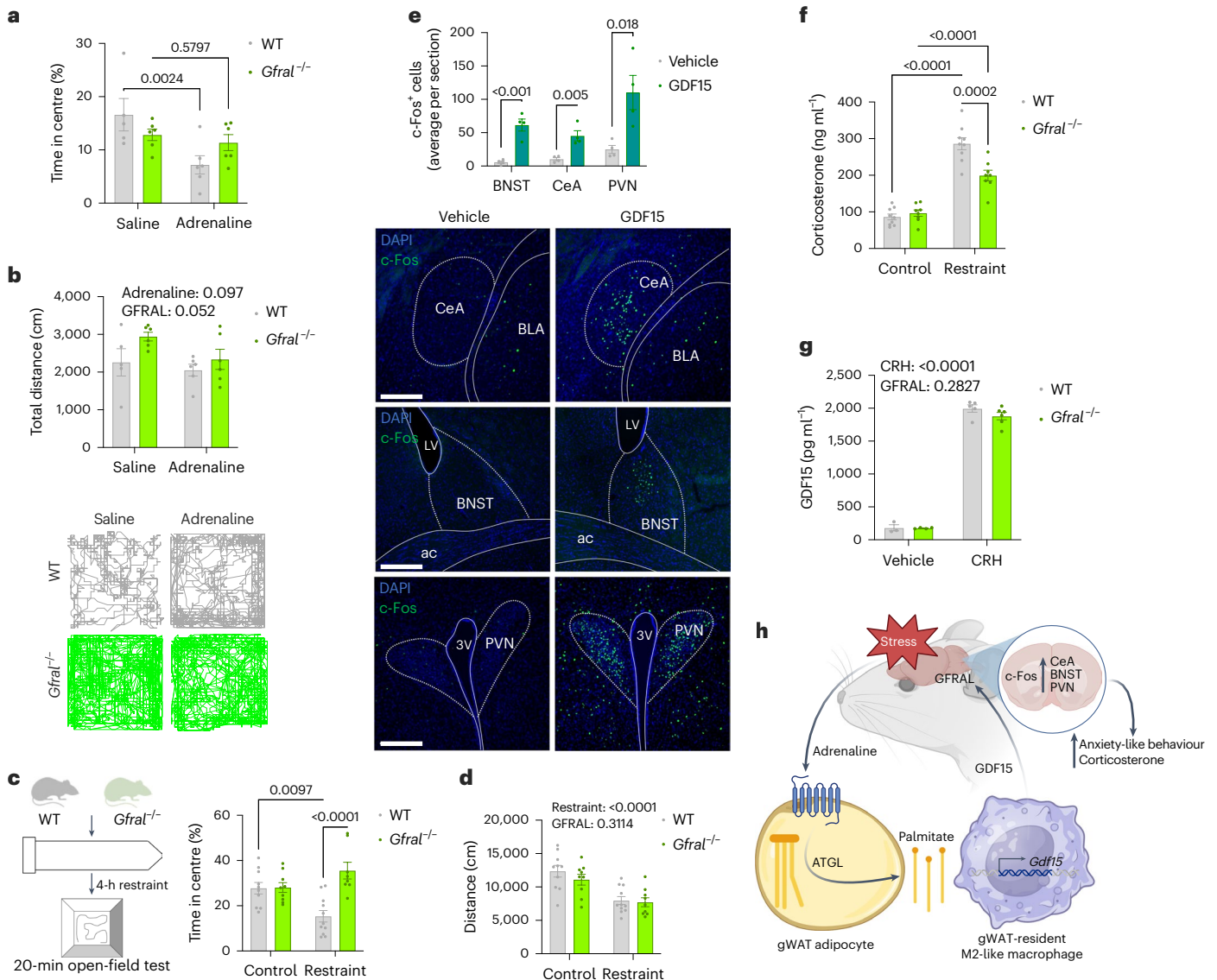


Fig. 4 | GDF15 regulates behavioural and physiological responses to acute psychological stress through multiple anxiogenic brain regions. **a**, Time in the centre during the open-field test following treatment with saline (WT $n = 5$ mice, $Gfral^{-/-}$ $n = 6$) or adrenaline (WT $n = 6$, $Gfral^{-/-}$ $n = 6$). Data are presented as mean \pm s.e.m. with P values calculated using a two-way ANOVA with post hoc testing and Tukey's correction. **b**, Top: total movement during the open-field test following treatment with saline (WT $n = 5$, $Gfral^{-/-}$ $n = 6$) or adrenaline (WT $n = 6$, $Gfral^{-/-}$ $n = 6$). Bottom: representative images of movements of individual mice. Data are presented as mean \pm s.e.m. with P values calculated using a two-way ANOVA with post hoc testing and Tukey's correction. **c**, Left: schematic of the acute restraint test. Right: time in the centre during the open-field test following 4 h of tube restraint (WT $n = 11$ mice, $Gfral^{-/-}$ $n = 8$) or the control condition (WT $n = 10$, $Gfral^{-/-}$ $n = 9$). Data are presented as mean \pm s.e.m. with P values calculated using a two-way ANOVA with post hoc testing and Tukey's correction. **d**, Total distance travelled during the open-field test following restraint (WT $n = 11$ mice, $Gfral^{-/-}$ $n = 9$) or the control condition (WT $n = 10$, $Gfral^{-/-}$ $n = 9$). Data are presented as mean \pm s.e.m. with P values calculated using a two-way ANOVA with post hoc testing and Tukey's correction. **e**, Top: quantification of c-Fos⁺ cells in the bed nucleus of the stria terminalis (BNST), central amygdala (CeA) and paraventricular nucleus of the hypothalamus (PVN) of mice 90 min following treatment with IP injected GDF15. Bottom: representative pictures of the staining ($n = 4$ per group). Data are presented as mean \pm s.e.m. with P values calculated using an unpaired two-tailed t test. Scale bar, 200 μ m. 3V, third ventricle; ac, anterior commissure; BLA, basolateral amygdala; LV, lateral ventricle. **f**, Serum corticosterone following restraint (WT $n = 9$ mice, $Gfral^{-/-}$ $n = 8$) or the control condition (WT $n = 9$, $Gfral^{-/-}$ $n = 8$). Data are presented as mean \pm s.e.m. with P values calculated using a two-way ANOVA with post hoc testing and Tukey's correction. **g**, Serum GDF15 after treatment with CRH (WT $n = 5$ mice, $Gfral^{-/-}$ $n = 6$) or vehicle (WT $n = 3$, $Gfral^{-/-}$ $n = 4$). Data are presented as mean \pm s.e.m. with P values calculated using a two-way ANOVA with post hoc testing and Tukey's correction. **h**, Schematic summary of the mechanism of GDF15-mediated anxiety-like behaviour. **h** created using BioRender.com.

anxiety-like behaviour in the open-field and light–dark box tests without affecting overall physical activity (Extended Data Fig. 7h,i). Critically, the anxiogenic effects of GDF15 persisted following repeated daily exposure, suggesting that tachyphylaxis did not occur (Extended Data Fig. 7j–l), similar to what we and others have shown for food intake and body weight loss with repeated GDF15 treatment^{26,54}.

Several brain regions are involved in the acute stress response^{2,3,55,56}. To determine the neurobiological substrates of GDF15-induced

$Gfral^{-/-}$ $n = 9$). Data are presented as mean \pm s.e.m. with P values calculated using a two-way ANOVA. **e**, Top: quantification of c-Fos⁺ cells in the bed nucleus of the stria terminalis (BNST), central amygdala (CeA) and paraventricular nucleus of the hypothalamus (PVN) of mice 90 min following treatment with IP injected GDF15. Bottom: representative pictures of the staining ($n = 4$ per group). Data are presented as mean \pm s.e.m. with P values calculated using an unpaired two-tailed t test. Scale bar, 200 μ m. 3V, third ventricle; ac, anterior commissure; BLA, basolateral amygdala; LV, lateral ventricle. **f**, Serum corticosterone following restraint (WT $n = 9$ mice, $Gfral^{-/-}$ $n = 8$) or the control condition (WT $n = 9$, $Gfral^{-/-}$ $n = 8$). Data are presented as mean \pm s.e.m. with P values calculated using a two-way ANOVA with post hoc testing and Tukey's correction. **g**, Serum GDF15 after treatment with CRH (WT $n = 5$ mice, $Gfral^{-/-}$ $n = 6$) or vehicle (WT $n = 3$, $Gfral^{-/-}$ $n = 4$). Data are presented as mean \pm s.e.m. with P values calculated using a two-way ANOVA with post hoc testing and Tukey's correction. **h**, Schematic summary of the mechanism of GDF15-mediated anxiety-like behaviour. **h** created using BioRender.com.

anxiogenesis, we measured *Fos*, an immediate early gene associated with neuronal activation, in several structures known to be involved in stress-related behaviours. The locus coeruleus is the main source of noradrenaline in the mammalian brain and is one of the first structures recruited following stressful stimuli^{3,4,57}. Given that GDF15's metabolic effects were recently shown to be dependent on β -adrenergic activity²⁶, the locus coeruleus represented a particularly relevant target. However, high-dose GDF15 did not increase c-Fos expression in locus coeruleus

noradrenergic neurons (Extended Data Fig. 8a) nor in the medial prefrontal cortex and basolateral amygdala, both downstream projections of the locus coeruleus known to drive anxiogenesis (Extended Data Fig. 8b)^{4,58}. In contrast, GDF15 showed increased activity in the central amygdala and the bed nucleus of the stria terminalis (Fig. 4e), each of which has well-established roles in anxiogenesis^{59–63}. Consistent with other studies, we also observed activation within the paraventricular nucleus of the hypothalamus (Fig. 4e)^{23,64}.

High levels of circulating GDF15 can activate corticotropin-releasing hormone (CRH) neurons within the paraventricular nucleus of the hypothalamus and activate the HPA axis, leading to the secretion of corticosterone in mice^{23,24,64}. We explored whether GDF15–GFRAL signalling is important for activating the HPA axis under more physiological conditions by applying physical restraint stress to WT and *Gfral*^{−/−} mice. Expectedly, restraint stress increased circulating corticosterone in both genotypes, reflecting activation of the HPA axis, but significantly less so in *Gfral*^{−/−} mice (Fig. 4f), despite circulating GDF15 levels being modestly elevated by restraint stress in both genotypes (Extended Data Fig. 8c). CRH is critical in driving stress-induced behavioural responses, such as anxiety and aversion^{3,50}. Intriguingly, exogenous CRH led to a marked increase in circulating GDF15 levels (Fig. 4g), further demonstrating the involvement of GDF15 and GFRAL in the stress response. Importantly, exogenous CRH increased adrenocorticotrophic hormone (ACTH) and corticosterone levels, whereas dexamethasone decreased corticosterone levels similarly in WT and *Gfral*^{−/−} mice, suggesting that there was no impairment in HPA axis signalling (Extended Data Fig. 8d–f).

Together, these data support the role of GDF15 in regulating acute stress-induced anxiety-like behaviour (Fig. 4h), possibly through the recruitment of multiple anxiogenic brain regions⁵⁶, and emphasize that GDF15–GFRAL signalling is transmitted broadly throughout the brain despite the brainstem-localized receptor expression.

Discussion

Mammals have evolved many mechanisms for detecting and avoiding noxious stimuli such as foodborne toxins, bacterial infections and allergens^{16,65–68}. GDF15 has been linked to all of these by inducing nausea, emesis (or pica) and aversive behaviour^{19,64,69}. However, in addition to physical stimuli, psychological stress produces its own set of physiological and behavioural responses intended to protect the organism. The fight-or-flight response is a classic example of psychological stress leading to metabolic responses that mobilize endogenous energy stores from adipose tissue^{13,70} and elicit behavioural responses such as anxiety^{5–9}. For decades, there has been evidence that adipose tissue lipolysis and peripheral adrenergic activity are associated with feelings of anxiety^{10–13}, but the link between these responses has remained elusive.

Here, we identified a mechanism whereby adrenergic activation of adipocyte lipolysis promotes the secretion of GDF15 from M2-like alternatively activated macrophages within adipose tissue, which, through its receptor, GFRAL, is critical for appropriate behavioural and physiological responses to acute psychological stress. These results are consistent with previous studies in which chronically supraphysiological levels of GDF15 promoted anxiety-like behaviour whereas lifelong deletion of GDF15 reduced anxiety^{21,22}. We also identified various anxiogenic brain regions, including the central amygdala, bed nucleus of the stria terminalis and paraventricular nucleus, that could be involved in mediating these responses. GDF15, at least at high circulating levels, has been shown to reduce physical activity^{71,72}, produce anxiety-like behaviour^{20–22} and activate the β -adrenergic^{25,26,68} and HPA axes^{23,24}. Indeed, optogenetic activation of GFRAL-expressing neurons is sufficient to activate the HPA axis and increase the circulating cortisol levels²⁴.

Clinical trials with GDF15 analogues did not report increases in anxiety^{73,74}. However, while our paper was in review, a study was published in which plasma proteomics conducted in individuals from the UK Biobank demonstrated that GDF15 is the circulating factor with the

strongest association with anxiety in humans compared with more than 3,000 other measured proteins⁷⁵. Herein, we show that GDF15–GFRAL signalling is a critical component of responses to acute psychological stress, including anxiety-like behaviour and HPA axis activation.

Some important limitations to the current data should be considered. First, the M1- and M2-like macrophage distinction is an oversimplification of the highly heterogeneous macrophage populations. Other publications have identified distinct macrophage subpopulations that secrete GDF15, at least in skeletal muscle⁷⁶, so it will be interesting to determine whether a particular subpopulation is responsible for the fatty acid-dependent secretion of GDF15 demonstrated here. Moreover, it will need to be determined how palmitate drives GDF15 secretion from macrophages and whether endogenous adipocyte-derived palmitate is sufficient to elicit this response. It is appealing to speculate that fatty acid-sensing PPARs, which have been shown to regulate GDF15 (ref. 47), could be involved, but this will need to be confirmed *in vivo*.

Despite the rapid increase in the rates of anxiety, there is a dearth of new targets for its treatment. The interactions between the brain and peripheral immune cells in the development of stress have been a growing area of interest^{77–79}, but previous studies have focused largely on classic inflammatory cytokines. Here, we provide additional insights into these interactions by identifying a new pathway for immune–brain crosstalk mediated by adrenergic-induced ATGL-dependent lipolysis and M2-like macrophage-secreted GDF15. These results raise the possibility that blocking GDF15–GFRAL signalling could mitigate acute stress-induced anxiety.

Methods

Mice

Germline GFRAL-knockout mice (*Gfral*^{−/−}) were generated as previously described, with breeding pairs provided by R. Seeley²⁶. Mice lacking β 1, β 2 and β 3 adrenergic receptors (*BR*^{−/−}) were generated as previously described^{26,80}. Adipocyte-specific ATGL-knockout animals were generated by crossing *Adipoq*-Cre mice with *Atgl/Pnpla2*-floxed mice⁸¹; *Atgl/Pnpla2*^{fllox/flox} littermates were used as controls. Animal studies were carried out at McMaster University (210104), the University of Toronto (21-467 and 24-0362H) or Washington University in St. Louis (20-0139). All animals used in the study were housed and cared for in accordance with the Guidelines for Animal Use at McMaster University and were approved by the McMaster University Animal Ethics Research Board or the ethics boards of their respective facilities. All mice were group-housed on a 12-h light–dark cycle with *ad libitum* access to food and water. The animals were housed either in a HEPA-filtered unit at room temperature or in specific pathogen-free microisolators at 29 °C and 40–60% relative humidity. Experiments were performed on mice at ages between 16 and 24 weeks. All mice were male unless stated otherwise, including for cell isolations.

Experiments were performed, and mice were killed in a fed state between 09:00 and 12:00. Terminal blood was collected by cardiac puncture, and blood from live animals (for example, time-course GDF15 levels) was collected from a tail vein. Blood samples were centrifuged at 8,000g for 10 min at 4 °C after clotting at room temperature for 30 min, and the supernatant was collected. Tissues were collected following anaesthetization with ketamine (75 mg kg^{−1}) and xylazine (10 mg kg^{−1}). Tissues were frozen at −80 °C until future analyses.

Male WT and *Gfral*^{−/−} mice were placed on a high-fat, high-fructose diet (40 kcal% fat (mostly palm oil), 20 kcal% fructose with 0.02% cholesterol; Research Diets, D19101102) starting at 12–20 weeks of age for 4 weeks. Palm oil (Sigma-Aldrich, 70905) was gavaged at 09:00 as described previously⁴⁹.

Mouse drug treatments

Adrenaline hydrochloride (Sigma-Aldrich, E4642) was diluted in saline and injected IP (09:00) at a dose of 0.5 mg per kg body weight based on previous studies^{82,83}. CL (Sigma-Aldrich, C5976) was diluted in saline and

injected IP (-09:00) at a dose of 1 mg per kg body weight⁸⁴. Cilostamide (Sigma-Aldrich, C7971; 10 mg per kg body weight, injected IP) was prepared in 10% DMSO and 5% Kolliphor⁸⁵. All control mice received saline IP injected at the same volume. Recombinant human GDF15 (5 nM kg⁻¹; Novo Nordisk) or vehicle was injected IP at -09:00 (ref. 26). To test for tachyphylaxis, we injected mice with either vehicle or GDF15 (5 nM kg⁻¹) for 9 days at -09:00. Chow diet was measured daily. On the 10th day, mice were injected with either vehicle or GDF15 (5 nM kg⁻¹), and open-field tests were performed 1 h later (described below). LPS (Sigma-Aldrich, O111:B4, L2630) was injected IP at a dose of 2 mg kg⁻¹ starting at 09:00, and control mice were injected with saline. CRH (Sigma-Aldrich, C3042) was injected IP at -09:00 at a dose of 90 µg kg⁻¹, and blood was collected from a tail vein at 0.5 and 3 h after injection⁸⁶. Dexamethasone (Sigma-Aldrich, D4902) was injected IP at -09:00 at a dose of 100 µg kg⁻¹, and blood was collected from a tail vein 6 h following injection⁸⁷.

Human paediatric anxiety samples

Children with obesity who were enrolled in the Canadian Pediatric Weight Management Registry at the McMaster site were included in this study. Study participants with an available fasting blood sample at their initial visit and a clinical diagnosis of anxiety but without antipsychotic or antidepressant medications ($n = 23$) were compared with those without any diagnosis of anxiety and also free from the use of medications ($n = 24$). Control participants and those with anxiety were matched for age (12.50 ± 2.97 and 12.44 ± 2.86 years), sex (12/11 and 12/12 male-to-female ratio), body weight (87 ± 31.88 and 88 ± 35.32 kg) and body mass index (33.18 ± 6.41 and 34.08 ± 8.07 kg m⁻²). Serum GDF15 was assessed from previously frozen samples in duplicate, as described below.

Separation of adipose tissue fractions

Each gWAT or iWAT sample was combined from two mice. WAT was collected, quickly rinsed in warm PBS, minced and incubated in collagenase (10 mM HEPES–Krebs–Ringer buffer, 4% BSA, 1.5 mg ml⁻¹ collagenase type I (Gibco, 17100017)) at 37 °C with gentle agitation for 30 min (gWAT) or 45 min (iWAT). Tissues were filtered (100 µm), and fractions were separated by repeated centrifugation at 500g for 5 min. F4/80⁺ cells were isolated using a commercially available kit as per the manufacturer's instructions (EasySep Mouse F4/80 Positive Selection Kit; STEMCELL Technologies, cat. no. 100-0659) along with an EasySep magnet (cat. no. 18000).

Adipocyte differentiation

Immortalized mouse white adipocytes were generated as previously described⁸⁸. Preadipocytes were grown to confluence in DMEM supplemented with 1% GlutaMAX, 1% penicillin–streptomycin, 10% FBS, insulin (20 nM) and T3 (1 nM; differentiation medium). Confluent cells were incubated for 48 h in differentiation medium further supplemented with isobutylmethylxanthine (0.5 mM), dexamethasone (0.5 µM) and indomethacin (0.125 mM; induction medium). All chemicals were from Sigma, and experiments were performed within 20 passages following immortalization.

Adipocytes were then treated with either CL (10 µM; Sigma-Aldrich, C5976), ATGListatin (40 µM; Sigma-Aldrich, SML1075), neither of the compounds (control) or a combination of the two compounds for 24 h in serum-free DMEM supplemented with 1% BSA (Sigma-Aldrich, cat. no. A8806). Medium was collected, and excess lipids and cellular debris were removed by centrifugation. Cells were washed with PBS and snap-frozen either in TRIzol for RNA extraction or in cell lysis buffer for protein content quantification using BCA. Lipolysis was assessed by measuring glycerol levels in the medium using a commercially available kit (Cayman Chemical, cat. no. 10010755).

BMDM isolation, differentiation and polarization

Femurs and tibias were collected from mice and cleaned of remaining muscle and soft tissues, and both ends of each bone were removed⁸⁹.

The bone marrow was extracted by centrifugation at 1,900g for 5 min. The marrow was resuspended in 1 ml DMEM (Wisent, cat. no. 319-005-CL, 25 mM glucose) and strained through a 40-µm cell strainer into a 50-ml Falcon tube. Cells were cultured for 4 h at 37 °C and 5% CO₂. After incubation, nonadherent cells were collected and combined with M-CSF (20 ng ml⁻¹; Peprotech, 315-02) to stimulate macrophage differentiation and plated for 7 days in DMEM (Wisent, cat. no. 319-005-CL) supplemented with FBS (10%, Wisent, cat. no. 098150) and penicillin–streptomycin (1%, Invitrogen). After differentiation, cells were washed, collected and plated onto 12-well plates (1×10^6 cells per ml) and left to adhere overnight.

Fully differentiated BMDMs were then polarized either with 100 ng ml⁻¹ LPS (Sigma-Aldrich, L2630) + 20 ng ml⁻¹ IFNγ (Peprotech, 315-05) to an M1-like phenotype or with 20 ng ml⁻¹ IL-4 (Peprotech, 214-14) to an M2-like phenotype for 24 h (ref. 42). Following polarization, cells were treated with either sodium palmitate (500 µM, Sigma-Aldrich, P9767), sodium oleate (500 µM, Sigma-Aldrich, O7501), tunicamycin (5 ng ml⁻¹, Cayman Chemical, 11089-65-9), rosiglitazone (1 µM; Sigma-Aldrich, R2408) or T0070907 (1 µM; Sigma-Aldrich, T8703) for another 24 h in DMEM (Wisent, 319-005-CL) supplemented with 1% fatty acid and endotoxin-free BSA (Sigma-Aldrich, cat. no. A8806). Medium was collected after 24 h and frozen at -80 °C until analysis. Cells were rinsed in PBS and collected either in TRIzol for RNA extraction (see below) or in cell lysis buffer for protein quantification using BCA.

RNA isolation, cDNA synthesis and qPCR

Tissues were homogenized in TRIzol reagent. An RNeasy kit (Qiagen, cat. no. 74106) was used for subsequent total RNA extraction and purification according to the manufacturer's instructions. cDNA synthesis was performed using the SuperScript IV Reverse Transcriptase kit (Invitrogen, cat. no. 18090010) following the manufacturer's instructions. cDNA expression for specific genes was detected by qPCR using the AmpliTaq Gold DNA Polymerase kit (Applied Biosystems, cat. no. N8080241). Relative mRNA levels were quantified with the ΔC_T method using mouse *Ppia* (Mm02342430_g1) as an endogenous control, except for adipocyte and SVF comparisons for which *Polr2a* was used (Mm00839502_m1). The gene-specific primers used were as follows: *Gdf15* (Mm00442228_m1), *Atf4* (Mm00515324_m1), *Chop/Ddit3* (Mm01135937_g1), *iNos* (Mm00440502_m1), *Arg1* (Mm00475988_m1), *Ppargc1a* (Mm01208835_m1), *Emr1/F480/Adgre1* (Mm00802529_m1), *Fgf21* (Mm07297622_g1), *Atgl/Pnpla2* (Mm00503040_m1) and *Lep* (Mm00434759_m1). All probes were purchased from Thermo Fisher.

RNA-seq and analyses

For RNA-seq, mice were injected with adrenaline (0.5 mg kg⁻¹ IP at 09:00) and gWAT was collected after 1 h. RNA was extracted as described above. Raw RNA-seq FASTQ data were imported into Galaxy for quality control and processing steps. The FastQC tool was used to check read quality, and the Cutadapt tool was used to trim adaptor sequences and remove low-quality reads. The remaining reads were aligned to the mm10 *Mus musculus* reference genome with the HISAT2 tool and quantified with the featureCounts tool. These counts data were imported into R for differential expression analysis with the DESeq2 package to detect DEGs (adjusted *P*-value (*P*-adj) < 0.05). Principal component analysis was performed in R using variance stabilizing transformation (VST)-normalized data from the DESeq2 analysis. Pathway analysis was performed with the GSEA software in combination with MSigDB gene sets. A list of human genes encoding secreted proteins (ligands) was obtained from the HUGO Gene Nomenclature Committee website. Mouse genes orthologous to these human ligand-encoding genes were obtained using the g:Profiler tool. A heat map was created with DEGs belonging to this group of ligand-encoding genes in R with the pheatmap package, using z-scored VST-normalized data. These genes were also highlighted in a volcano plot, which was created with

the Enhanced Volcano package in R, using fold-change and *P*-adj values from the DESeq2 analysis.

Single-cell RNA-seq

The scRNA-seq data used for the analyses described in this article were obtained from the National Center for Biotechnology Information Sequence Read Archive under reference number [SRP145475](#) (ref. 40). Cell Ranger was used to perform sample qualification, alignment, filtering, counting and aggregation using the Linux system or R and RStudio software. Clustering and gene expression were visualized with the 10X Genomics Loupe Browser (v.6.5.0).

2SMR using GWAS summary data

2SMR was performed using the exposure and outcome from two non-overlapping and independent datasets to conduct the summary-level instrument–exposure analysis and the instrument–outcome association analysis. 2SMR was performed using the R package TwoSampleMR (v0.5.6)⁹⁰. To verify the causal effect of GDF15 on nerves, anxiety, tension or depression in humans, we performed 2SMR using the exposure dataset (GDF15, GWAS ID: ebi-a-GCST90011998, sample size: 21,758)^{91,92} and outcome dataset (nerves, anxiety, tension or depression, GWAS ID: ebi-a-GCST90013910, sample size: 407,746)⁹³. We identified genetic variants (single-nucleotide polymorphisms) associated with blood GDF15 protein levels in the GWAS catalogue dataset based on cis-protein quantitative trait loci (within 500 kb of the *Gdf15* gene) and further selected proxy single-nucleotide polymorphisms by linkage disequilibrium clumping ($P_1 = 5 \times 10^{-8}$, clump = TRUE, $P_2 = 1 \times 10^{-7}$, $r_2 = 0.01$, kb = 10,000). After dropping duplicate exposure–outcome summary sets, we further performed sensitivity analyses, including heterogeneity statistics, horizontal pleiotropy and leave-one-out analysis. After confirming that there was no heterogeneity or horizontal pleiotropy, we next performed Mendelian randomization analysis and visualized the results using the scatter plot and forest plot functions in the R package TwoSampleMR. The inverse-variance weighted method was used to assess the significance of the causal effect of the exposure on the outcome. 2SMR was performed using R and RStudio.

Serum and medium analyses

Serum and cell-based GDF15 levels were measured by ELISA (R&D Systems, DY6385) as per the manufacturer's instructions^{18,45}. Serum corticosterone (Thermo Fisher, EIACORT), adrenocorticotropic hormone (Abcam, ab263880) and adrenaline (Abnova, KA1882) were measured following the manufacturer's instructions.

c-Fos immunofluorescence and quantification

C57BL/6J mice were injected with GDF15 (5 nM kg⁻¹) or vehicle; 90 min later, the mice were anaesthetized with a mixture of ketamine (69.57 mg ml⁻¹), xylazine (4.35 mg ml⁻¹) and acepromazine (0.87 mg ml⁻¹) IP and perfused with 10 ml of 0.1 M phosphate buffer (PB) followed by 25 ml of 4% paraformaldehyde (PFA) in 0.1 MPB. The brains were removed, postfixed overnight (4% PFA in 0.1 MPB) and kept at 4 °C in 30% sucrose solution until cutting. Coronal sections (40 µm) were obtained using a microtome (Leica SM 2000R) and serially collected in PBS. Sections were washed in PBS (3 × 10 min) and preincubated in PBS containing Triton X-100 (0.3%) and normal goat serum (5%) for 1 h. Sections were then incubated overnight at room temperature in PBS containing Triton X-100 (0.3%), normal goat serum (1%) and rabbit anti-c-Fos (1:1,000, Cell Signaling Technology). Sections were then washed in PBS (3 × 10 min), incubated with Alexa Fluor 488 goat anti-rabbit secondary antibody (1:400, Invitrogen) in PBS containing Triton X-100 (0.3%) and normal goat serum (1%) for 2 h, and washed in PBS (3 × 10 min). Sections were finally serially mounted in Vectashield medium with DAPI (Vector Laboratories). Image acquisition was performed using Zeiss Axio Scan 7.

Western blotting

Proteins were extracted using lysis buffer containing 50 mM HEPES (pH 7.4), 150 mM NaCl, 100 mM NaF, 10 sodium pyrophosphate, 5 mM EDTA, 250 mM sucrose, 1 mM DTT, 1 mM sodium orthovanadate, 1% Triton X-100 and cOmplete Protease Inhibitor Cocktail (Roche). The total protein concentration in the samples was measured by the BCA protein assay. Protein concentrations were adjusted and diluted in 4× SDS sample buffer. Proteins were separated using SDS–PAGE gels and transferred to poly(vinylidene difluoride) membranes. After blocking for 1 h with 5% BSA in TBST at room temperature, membranes were incubated with the primary antibodies overnight at 4 °C (phosphorylated PKA substrates (1:1,000, Cell Signalling #9624) or tubulin (1:1,000, Abcam #ab4074)). After washing, membranes were incubated with a secondary antibody at room temperature for 1 h. Protein bands were visualized with the Fusion FX7 system (MBI) and quantified using ImageJ software.

Tube restraint and stress tests

Mice were put into 50-ml Falcon tubes (beginning at -09:00) with holes at both ends so the tail was exposed and there was sufficient air flow³. Control mice remained in their home cage with food and water removed at the initiation of tube restraint. Immediately following tube restraint, mice were either anaesthetized for tissue collection or submitted to open-field test protocols (see below).

Alternatively, social isolation was induced by individually housing previously group-housed mice for 3 days and comparing them with their continually group-housed littermates³¹. In the cage-switch model, mice were removed from their home cage and placed in an identical cage with the dirty bedding of nonlittermate males³¹. Nondisturbed socially housed littermates were applied as the controls.

To assess stress-induced food intake and nausea, we provided mice with kaolin clay (Research Diets, K50001) in addition to their regular diet for 3 days before testing. Mice were restrained (starting at -09:00) for 4 h and returned to their cages (group-housed) with access to standard chow and kaolin clay pellets, which were weighed before and after 18 h (-09:00 the following day).

Open-field and light–dark box tests

Mice were moved to an isolated room the evening before open-field testing to minimize stress on the day of testing. Immediately following 4-h tube restraint or 1 h following exogenous GDF15 injection (5 nM kg⁻¹ IP) or 1 h following exogenous adrenaline treatment (0.5 mg kg⁻¹ IP), mice were placed in the centre of a box (40 × 40 × 40 cm, black walls and white plastic bottom). Mice remained in the box in the same isolated room, and videos were recorded using a camera (GoPro, 1080p resolution and a sample rate of 3 frames per second) mounted to the ceiling. Videos were recorded for 20 min. The two-dimensional mouse pose was analysed using DeepLabCut⁹⁴ to extract the locations of arena boundaries and anatomical landmarks (nose, left ear, right ear, tail base). The DeepLabCut model (ResNet50 architecture) was trained using 20 distinct frames (*k*-means clustering) from 20 input videos for a total of 200,000 epochs, resulting in a mean testing error of 3.74 pixels across all tracked positional landmarks. Weighted spatial means of all four anatomical points taken to represent the location of the centre of the head were then analysed using custom MATLAB (v2022b) scripts for the time spent in the centre (>8 cm from the arena boundaries), time spent in the periphery (<8 cm from one arena boundary), time spent in the corners (<8 cm from two arena boundaries) and total distance moved during the test. Afterwards, the mice were returned to their home cages, and the boxes were thoroughly cleaned and left to dry before subsequent rounds. The boxes in which groups (that is, WT/GFRAL, control/restraint, control/GDF15, etc.) were placed were systematically rotated to control for any possible differences in box positioning during recording. Alternatively, mice were placed into an automated open-field test system (Opto-Varimex-5 Auto-Track, Columbus Instruments) for 20 min, and the time spent in the centre and periphery and the total movement were analysed using equipment software.

For light–dark box testing, mice were placed into the ‘light’ area and videos were recorded using a camera (GoPro, 1080p resolution and a sample rate of 3 frames per second) for 10 min. The videos were analysed manually by a blinded assessor for the time spent by the mice in the light area.

Behavioural and metabolic activity

Metabolic and behavioural monitoring was conducted using the Promethion system (Sable Systems International). Data were collected following acclimation to the system for 24 h. After acclimation, mice were injected with adrenaline (0.5 mg kg⁻¹ IP) at 09:00, after which the mice remained in the system for another 24 h. Data on food intake, physical activity and nonambulatory movements (beam breaks), oxygen consumption (VO₂), carbon dioxide production (VCO₂), respiratory exchange ratio (VCO₂/VO₂) and energy expenditure (kcal h⁻¹) were collected at 15-min intervals.

Statistics

Statistical analyses were performed using GraphPad Prism (version 10) or R software (RNA-seq). Data were analysed using an unpaired *t* test, a one-way analysis of variance (ANOVA) or a two-way ANOVA. When significant interactions were detected through ANOVA, subsequent post hoc analyses were reported with appropriate corrections; where no post hoc correction is stated, there was no interaction detected. Correlational analyses were performed with Pearson’s correlation. No statistical methods were used to predetermine sample sizes, but our sample sizes are similar to those reported in previous publications^{18,26}. Normality was tested using the Shapiro–Wilk test. Outliers were defined as points outside 2 s.d. away from the group mean. All data are presented as mean ± s.e.m. with individual data points. Differences were considered significant when *P* < 0.05.

Reporting summary

Further information on research design is available in the Nature Portfolio Reporting Summary linked to this article.

Data availability

Data that support the findings of this study are available from the corresponding author on request. Bulk RNA-seq data have been deposited under accession code [GSE267183](#). scRNA-seq data were obtained from the National Center for Biotechnology Information Sequence Read Archive reference number [SRP145475](#). Source data are provided with this paper.

Code availability

The code for RNA-seq analysis and 2SMR is available on request.

References

- Kessler, R. C., Chiu, W. T., Demler, O., Merikangas, K. R. & Walters, E. E. Prevalence, severity, and comorbidity of 12-month DSM-IV disorders in the National Comorbidity Survey Replication. *Arch. Gen. Psychiatry* **62**, 617–627 (2005).
- Ulrich-Lai, Y. M. & Herman, J. P. Neural regulation of endocrine and autonomic stress responses. *Nat. Rev. Neurosci.* **10**, 397–409 (2009).
- McCall, J. G. et al. CRH engagement of the locus coeruleus noradrenergic system mediates stress-induced anxiety. *Neuron* **87**, 605–620 (2015).
- McCall, J. G. et al. Locus coeruleus to basolateral amygdala noradrenergic projections promote anxiety-like behavior. *eLife* **6**, e18247 (2017).
- Burns, T. W., Mohs, J. M., Langley, P. E., Yawn, R. & Chase, G. R. Regulation of human lipolysis. In vivo observations on the role of adrenergic receptors. *J. Clin. Invest.* **53**, 338–341 (1974).
- Elmadjian, F., Hope, J. M. & Lamson, E. T. Excretion of epinephrine and norepinephrine in various emotional states. *J. Clin. Endocrinol. Metab.* **17**, 608–620 (1957).
- Pollin, W. & Goldin, S. The physiological and psychological effects of intravenously administered epinephrine and its metabolism in normal and schizophrenic men. II. Psychiatric observations. *J. Psychiatr. Res.* **1**, 50–67 (1961).
- Clayton, E. C. & Williams, C. L. Noradrenergic receptor blockade of the NTS attenuates the mnemonic effects of epinephrine in an appetitive light–dark discrimination learning task. *Neurobiol. Learn. Mem.* **74**, 135–145 (2000).
- King, S. O. 2nd & Williams, C. L. Novelty-induced arousal enhances memory for cued classical fear conditioning: interactions between peripheral adrenergic and brainstem glutamatergic systems. *Learn. Mem.* **16**, 625–634 (2009).
- Gottschalk, L. A., Stone, W. N. & Gleser, G. C. Peripheral versus central mechanisms accounting for antianxiety effects of propranolol. *Psychosom. Med.* **36**, 47–56 (1974).
- Stone, W. N., Gleser, G. C. & Gottschalk, L. A. Anxiety and β -adrenergic blockade. *Arch. Gen. Psychiatry* **29**, 620–622 (1973).
- Flemenbaum, A. Cyclic AMP, alpha and beta receptors as a further explanation of the propranolol–FFA activity. *Psychosom. Med.* **37**, 74 (1975).
- Gottschalk, L. A., Stone, W. N., Gleser, G. C. & Iacono, J. M. Anxiety levels in dreams: relation to changes in plasma free fatty acids. *Science* **153**, 654–657 (1966).
- Bonn, J. A., Turner, P. & Hicks, D. C. Beta-adrenergic-receptor blockade with practolol in treatment of anxiety. *Lancet* **1**, 814–815 (1972).
- Wang, D. et al. GDF15: emerging biology and therapeutic applications for obesity and cardiometabolic disease. *Nat. Rev. Endocrinol.* **17**, 592–607 (2021).
- Lockhart, S. M., Saudek, V. & O’Rahilly, S. GDF15: a hormone conveying somatic distress to the brain. *Endocr. Rev.* **41**, bnaa007 (2020).
- Yang, L. et al. GFRAL is the receptor for GDF15 and is required for the anti-obesity effects of the ligand. *Nat. Med.* **23**, 1158–1166 (2017).
- Day, E. A. et al. Metformin-induced increases in GDF15 are important for suppressing appetite and promoting weight loss. *Nat. Metab.* **1**, 1202–1208 (2019).
- Borner, T. et al. GDF15 induces an aversive visceral malaise state that drives anorexia and weight loss. *Cell Rep.* **31**, 107543 (2020).
- Worth, A. A. et al. The cytokine GDF15 signals through a population of brainstem cholecystokinin neurons to mediate anorectic signalling. *eLife* **9**, e55164 (2020).
- Gil, C. I. et al. Mitochondrial stress-induced GFRAL signaling controls diurnal food intake and anxiety-like behavior. *Life Sci. Alliance* **5**, e202201495 (2022).
- Low, J. K. et al. First behavioural characterisation of a knockout mouse model for the transforming growth factor (TGF)- β superfamily cytokine, MIC-1/GDF15. *PLoS ONE* **12**, e0168416 (2017).
- Cimino, I. et al. Activation of the hypothalamic–pituitary–adrenal axis by exogenous and endogenous GDF15. *Proc. Natl Acad. Sci. USA* **118**, e2106868118 (2021).
- Ruud, L. E. et al. Activation of GFRAL⁺ neurons induces hypothermia and glucoregulatory responses associated with nausea and torpor. *Cell Rep.* **43**, 113960 (2024).
- Sjoberg, K. A. et al. GDF15 increases insulin action in the liver and adipose tissue via a β -adrenergic receptor-mediated mechanism. *Cell Metab.* **35**, 1327–1340 (2023).
- Wang, D. et al. GDF15 promotes weight loss by enhancing energy expenditure in muscle. *Nature* **619**, 143–150 (2023).

27. Stone, W. N., Gleser, G. C., Gottschalk, L. A. & Iacono, J. M. Stimulus, affect, and plasma free fatty acid. *Psychosom. Med.* **31**, 331–341 (1969).
28. Williams, T. & Williams, C. L. Peripheral arousal-related hormones modulate norepinephrine release in the hippocampus via influences on brainstem nuclei. *Behav. Brain Res.* **153**, 87–95 (2004).
29. Markussen, L. K. et al. Lipolysis regulates major transcriptional programs in brown adipocytes. *Nat. Commun.* **13**, 3956 (2022).
30. Bruford, E. A. et al. Guidelines for human gene nomenclature. *Nat. Genet.* **52**, 754–758 (2020).
31. Qing, H. et al. Origin and function of stress-induced IL-6 in murine models. *Cell* **182**, 1660 (2020).
32. Karusheva, Y. et al. The common H202D variant in GDF-15 does not affect its bioactivity but can significantly interfere with measurement of its circulating levels. *J. Appl. Lab. Med.* **7**, 1388–1400 (2022).
33. Jeong, K. H. et al. Impaired basal and restraint-induced epinephrine secretion in corticotropin-releasing hormone-deficient mice. *Endocrinology* **141**, 1142–1150 (2000).
34. Lafontan, M. & Berlan, M. Fat cell adrenergic receptors and the control of white and brown fat cell function. *J. Lipid Res.* **34**, 1057–1091 (1993).
35. Patel, A. R. et al. LPS induces rapid increase in GDF15 levels in mice, rats, and humans but is not required for anorexia in mice. *Am. J. Physiol. Gastrointest. Liver Physiol.* **322**, G247–G255 (2022).
36. Haemmerle, G. et al. Defective lipolysis and altered energy metabolism in mice lacking adipose triglyceride lipase. *Science* **312**, 734–737 (2006).
37. Zhou, C. et al. Sympathetic overdrive and unrestrained adipose lipolysis drive alcohol-induced hepatic steatosis in rodents. *Mol. Metab.* **78**, 101813 (2023).
38. Mayer, N. et al. Development of small-molecule inhibitors targeting adipose triglyceride lipase. *Nat. Chem. Biol.* **9**, 785–787 (2013).
39. L'Homme, L. et al. Adipose tissue macrophage infiltration and hepatocyte stress increase GDF-15 throughout development of obesity to MASH. *Nat. Commun.* **15**, 7173 (2024).
40. Burl, R. B. et al. Deconstructing adipogenesis induced by β 3-adrenergic receptor activation with single-cell expression profiling. *Cell Metab.* **28**, 300–309 (2018).
41. Caputa, G., Castoldi, A. & Pearce, E. J. Metabolic adaptations of tissue-resident immune cells. *Nat. Immunol.* **20**, 793–801 (2019).
42. Morgan, P. K. et al. Macrophage polarization state affects lipid composition and the channeling of exogenous fatty acids into endogenous lipid pools. *J. Biol. Chem.* **297**, 101341 (2021).
43. Abe, I. et al. Lipolysis-derived linoleic acid drives beige fat progenitor cell proliferation. *Dev. Cell* **57**, 2623–2637 (2022).
44. Townsend, L. K. et al. High-saturated-fat diet-induced obesity causes hepatic interleukin-6 resistance via endoplasmic reticulum stress. *J. Lipid Res.* **60**, 1236–1249 (2019).
45. Townsend, L. K. et al. AMPK mediates energetic stress-induced liver GDF15. *FASEB J.* **35**, e21218 (2021).
46. Kratz, M. et al. Metabolic dysfunction drives a mechanistically distinct proinflammatory phenotype in adipose tissue macrophages. *Cell Metab.* **20**, 614–625 (2014).
47. Lu, J. F. et al. GDF15 is a major determinant of ketogenic diet-induced weight loss. *Cell Metab.* **35**, 2165–2182 (2023).
48. Fulton, S., Décarie-Spain, L., Fioramonti, X., Guiard, B. & Nakajima, S. The menace of obesity to depression and anxiety prevalence. *Trends Endocrinol. Metab.* **33**, 18–35 (2022).
49. Wang, D. et al. Fatty acids increase GDF15 and reduce food intake through a GFRAL signaling axis. *Diabetes* **73**, 51–56 (2024).
50. Füzesi, T. et al. Hypothalamic CRH neurons orchestrate complex behaviours after stress. *Nat. Commun.* **7**, 11937 (2016).
51. Bales, M. B. et al. High fat diet blunts stress-induced hypophagia and activation of GIPr dorsal lateral septum neurons in male but not in female mice. *Mol. Metab.* **64**, 101571 (2022).
52. Holt, M. K. et al. Preproglucagon neurons in the nucleus of the solitary tract are the main source of brain GLP-1, mediate stress-induced hypophagia, and limit unusually large intakes of food. *Diabetes* **68**, 21–33 (2019).
53. Fortin, S. M. et al. The locus coeruleus contributes to the anorectic, nausea, and autonomic physiological effects of glucagon-like peptide-1. *Sci. Adv.* **9**, eadh0980 (2023).
54. Hsu, J.-Y. et al. Non-homeostatic body weight regulation through a brainstem-restricted receptor for GDF15. *Nature* **550**, 255–259 (2017).
55. Niu, M. et al. Claustrum mediates bidirectional and reversible control of stress-induced anxiety responses. *Sci. Adv.* **8**, eabi6375 (2022).
56. Calhoun, G. G. & Tye, K. M. Resolving the neural circuits of anxiety. *Nat. Neurosci.* **18**, 1394–1404 (2015).
57. Chandler, D. J. et al. Redefining noradrenergic neuromodulation of behavior: impacts of a modular locus coeruleus architecture. *J. Neurosci.* **39**, 8239–8249 (2019).
58. Hirschberg, S., Li, Y., Randall, A., Kremer, E. J. & Pickering, A. E. Functional dichotomy in spinal- vs prefrontal-projecting locus coeruleus modules splits descending noradrenergic analgesia from ascending aversion and anxiety in rats. *eLife* **6**, e29808 (2017).
59. Kim, S.-Y. et al. Diverging neural pathways assemble a behavioural state from separable features in anxiety. *Nature* **496**, 219–223 (2013).
60. Cowley, N. A. et al. Dynorphin controls the gain of an amygdalar anxiety circuit. *Cell Rep.* **14**, 2774–2783 (2016).
61. Gipelin, N. W., Herman, M. A. & Roberto, M. The central amygdala as an integrative hub for anxiety and alcohol use disorders. *Biol. Psychiatry* **77**, 859–869 (2015).
62. Borodovitsyna, O., Duffy, B. C., Pickering, A. E. & Chandler, D. J. Anatomically and functionally distinct locus coeruleus efferents mediate opposing effects on anxiety-like behavior. *Neurobiol. Stress* **13**, 100284 (2020).
63. Sun, Y., Qian, L., Xu, L., Hunt, S. & Sah, P. Somatostatin neurons in the central amygdala mediate anxiety by disinhibition of the central subnucleus extended amygdala. *Mol. Psychiatry* **28**, 4163–4174 (2023).
64. Sabatini, P. V. et al. GFRAL-expressing neurons suppress food intake via aversive pathways. *Proc. Natl Acad. Sci. USA* **118**, e2021357118 (2021).
65. O'Rahilly, S. GDF15—from biomarker to allostatic hormone. *Cell Metab.* **26**, 807–808 (2017).
66. Patel, S. et al. GDF15 provides an endocrine signal of nutritional stress in mice and humans. *Cell Metab.* **29**, 707–718 (2019).
67. Florsheim, E. B. et al. Immune sensing of food allergens promotes avoidance behaviour. *Nature* **620**, 643–650 (2023).
68. Luan, H. H. et al. GDF15 is an inflammation-induced central mediator of tissue tolerance. *Cell* **178**, 1231–1244 (2019).
69. Borner, T. et al. GDF15 induces anorexia through nausea and emesis. *Cell Metab.* **31**, 351–362 (2020).
70. Lönnqvist, F., Wennlund, A., Wahrenberg, H. & Arner, P. Effects of mental stress on lipolysis in humans. *Metabolism* **41**, 622–630 (1992).
71. Klein, A. B. et al. Pharmacological but not physiological GDF15 suppresses feeding and the motivation to exercise. *Nat. Commun.* **12**, 1041 (2021).
72. Macia, L. et al. Macrophage inhibitory cytokine 1 (MIC-1/GDF15) decreases food intake, body weight and improves glucose tolerance in mice on normal & obesogenic diets. *PLoS ONE* **7**, e34868 (2012).

73. Benichou, O. et al. Discovery, development, and clinical proof of mechanism of LY3463251, a long-acting GDF15 receptor agonist. *Cell Metab.* **35**, 274–286 (2023).
74. Zhang, Y. et al. Activity-balanced GLP-1/GDF15 dual agonist reduces body weight and metabolic disorder in mice and non-human primates. *Cell Metab.* **35**, 287–298 (2023).
75. Deng, Y.-T. et al. Atlas of the plasma proteome in health and disease in 53,026 adults. *Cell* **188**, 253–271 (2025).
76. Patsalos, A. et al. A growth factor-expressing macrophage subpopulation orchestrates regenerative inflammation via GDF-15. *J. Exp. Med.* **219**, e20210420 (2022).
77. Irwin, M. R. & Cole, S. W. Reciprocal regulation of the neural and innate immune systems. *Nat. Rev. Immunol.* **11**, 625–632 (2011).
78. Glaser, R. & Kiecolt-Glaser, J. K. Stress-induced immune dysfunction: implications for health. *Nat. Rev. Immunol.* **5**, 243–251 (2005).
79. Le Thuc, O. & García-Cáceres, C. Obesity-induced inflammation: connecting the periphery to the brain. *Nat. Metab.* **6**, 1237–1252 (2024).
80. Bachman, E. S. et al. β AR signaling required for diet-induced thermogenesis and obesity resistance. *Science* **297**, 843–845 (2002).
81. Kaur, S. et al. Adipose-specific ATGL ablation reduces burn injury-induced metabolic derangements in mice. *Clin. Transl. Med.* **11**, e417 (2021).
82. Dibe, H. A., Townsend, L. K., McKie, G. L. & Wright, D. C. Epinephrine responsiveness is reduced in livers from trained mice. *Physiol. Rep.* **8**, e14370 (2020).
83. Pedersen, L. et al. Voluntary running suppresses tumor growth through epinephrine- and IL-6-dependent NK cell mobilization and redistribution. *Cell Metab.* **23**, 554–562 (2016).
84. Townsend, L. K. et al. Loss of glucagon signaling alters white adipose tissue browning. *FASEB J.* **33**, 4824–4835 (2019).
85. Medak, K. D., McKie, G. L., Shamshoum, H., Seguin, I. & Wright, D. C. The glucose lowering effects of CL 316,243 dissipate with repeated use and are rescued by cilostamide. *Physiol. Rep.* **10**, e15187 (2022).
86. Muglia, L. J. et al. Corticotropin-releasing hormone links pituitary adrenocorticotropin gene expression and release during adrenal insufficiency. *J. Clin. Invest.* **105**, 1269–1277 (2000).
87. Laryea, G., Schütz, G. & Muglia, L. J. Disrupting hypothalamic glucocorticoid receptors causes HPA axis hyperactivity and excess adiposity. *Mol. Endocrinol.* **27**, 1655–1665 (2013).
88. Mottillo, E. P. et al. Lack of adipocyte AMPK exacerbates insulin resistance and hepatic steatosis through brown and beige adipose tissue function. *Cell Metab.* **24**, 118–129 (2016).
89. Galic, S. et al. Hematopoietic AMPK β 1 reduces mouse adipose tissue macrophage inflammation and insulin resistance in obesity. *J. Clin. Invest.* **121**, 4903–4915 (2011).
90. Hemani, G. et al. The MR-Base platform supports systematic causal inference across the human genome. *eLife* **7**, e34408 (2018).
91. Taliun, S. A. G. & Evans, D. M. Ten simple rules for conducting a Mendelian randomization study. *PLoS Comput. Biol.* **17**, e1009238 (2021).
92. Sanderson, E. et al. Mendelian randomization. *Nat. Rev. Methods Primers* **2**, 6 (2022).
93. Liu, Y. et al. Genetic architecture of 11 organ traits derived from abdominal MRI using deep learning. *eLife* **10**, e65554 (2021).
94. Nath, T. et al. Using DeepLabCut for 3D markerless pose estimation across species and behaviors. *Nat. Protoc.* **14**, 2152–2176 (2019).

Acknowledgements

G.R.S. acknowledges the support of a Diabetes Canada Investigator Award (OG-3-22-5645-GS), a Canadian Institutes of Health Research

(CIHR) Foundation Grant (201709FDN-CEBA-116200), a Tier 1 Canada Research Chair in Metabolic Diseases and a J. Bruce Duncan Endowed Chair in Metabolic Diseases. L.K.T. acknowledges the support of a CIHR Post-doctoral Fellowship Award, a Michael DeGroote Fellowship Award in Basic Biomedical Science and a MITACS fellowship supported by Novo Nordisk. D.W. acknowledges the support of fellowship grants from the McMaster Institute for Research on Aging (MIRA) at McMaster University. E.M.D. acknowledges the support of a Vanier Canada Graduate Scholarship. A.M. was supported by the Natural Sciences and Engineering Research Council of Canada. D.P.B. acknowledges the support of the GSK Chair in Diabetes of Université de Sherbrooke and an FRQS J1 salary award. A.C.C. acknowledges the support of a Tier 1 Canada Research Chair in Molecular Imaging of Diabetes and a CIHR Grant (no. 299962). J.G.M. acknowledges the support of a National Institutes of Health award (R01NS117899).

Author contributions

The overall conceptualization of studies included in this work was done by L.K.T. and G.R.S. Mouse experiments were designed, managed, performed and analysed by L.K.T., D.W., C.M.K., K.D.M., D.M.M., E.M.D., Z.P., E.E.T., J.L., A.E.P., O.I. and C.M.V. RNA-seq analyses were performed by D.W. and R.F. Mouse behaviour studies were done with the assistance of A.M., S.M.B. and R.E.K.M. c-Fos staining experiments were designed, managed, performed and analysed by L.J.B. and J.G.M. Adipocyte and macrophage experiments were completed by L.K.T., E.E.T., E.M.D., Z.P. and C.M.V. L.K.T. and G.R.S. wrote the paper, with the assistance of J.G.M., M.G.J., A.C.C., D.P.B., K.M.M., J.D.S. and D.C.W. The paper was reviewed, edited and approved by all the authors.

Competing interests

G.R.S. is a cofounder and shareholder of Espervita Therapeutics, a company developing new medications for fibrosis and cancer. McMaster University has received funding from Cambrian Biosciences, Catalym, Espervita Therapeutics, Esperion Therapeutics, Merck, Nestle, Novo Nordisk and Poxel Pharmaceuticals for research conducted in the laboratory of G.R.S. G.R.S. has received consulting and speaking fees from AstraZeneca, CurieBio, Eli Lilly, Esperion Therapeutics, Korro Bio, Keros Therapeutics, Merck, Novo Nordisk, Versant Ventures and Poxel Pharmaceuticals. A.C.C. received consulting and speaking fees from Eli Lilly, HLS Therapeutics, Janssen, Novartis Pharmaceuticals Canada and Novo Nordisk Canada. The other authors declare no competing interests.

Additional information

Extended data is available for this paper at <https://doi.org/10.1038/s42255-025-01264-3>.

Supplementary information The online version contains supplementary material available at <https://doi.org/10.1038/s42255-025-01264-3>.

Correspondence and requests for materials should be addressed to Gregory R. Steinberg.

Peer review information *Nature Metabolism* thanks Mónica Moreira-Rodrigues and the other, anonymous, reviewer(s) for their contribution to the peer review of this work. Primary Handling Editor: Christoph Schmitt, in collaboration with the *Nature Metabolism* team.

Reprints and permissions information is available at www.nature.com/reprints.

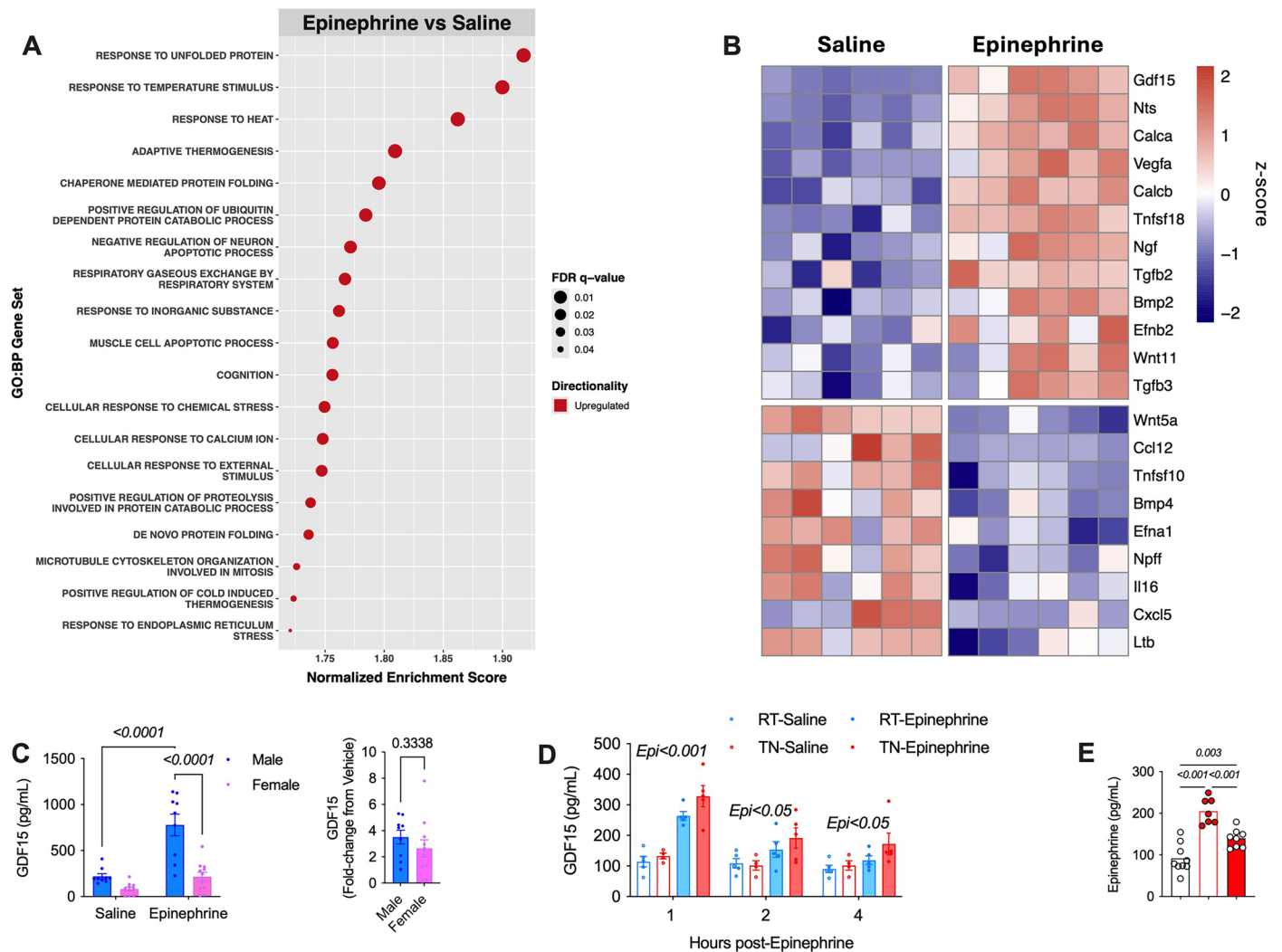
Publisher's note Springer Nature remains neutral with regard to jurisdictional claims in published maps and institutional affiliations.

Open Access This article is licensed under a Creative Commons Attribution-NonCommercial-NoDerivatives 4.0 International License, which permits any non-commercial use, sharing, distribution and reproduction in any medium or format, as long as you give appropriate credit to the original author(s) and the source, provide a link to the Creative Commons licence, and indicate if you modified the licensed material. You do not have permission under this licence to share adapted material derived from this article or parts of it. The images or other third party material in this article are included in the article's

Creative Commons licence, unless indicated otherwise in a credit line to the material. If material is not included in the article's Creative Commons licence and your intended use is not permitted by statutory regulation or exceeds the permitted use, you will need to obtain permission directly from the copyright holder. To view a copy of this licence, visit <http://creativecommons.org/licenses/by-nc-nd/4.0/>.

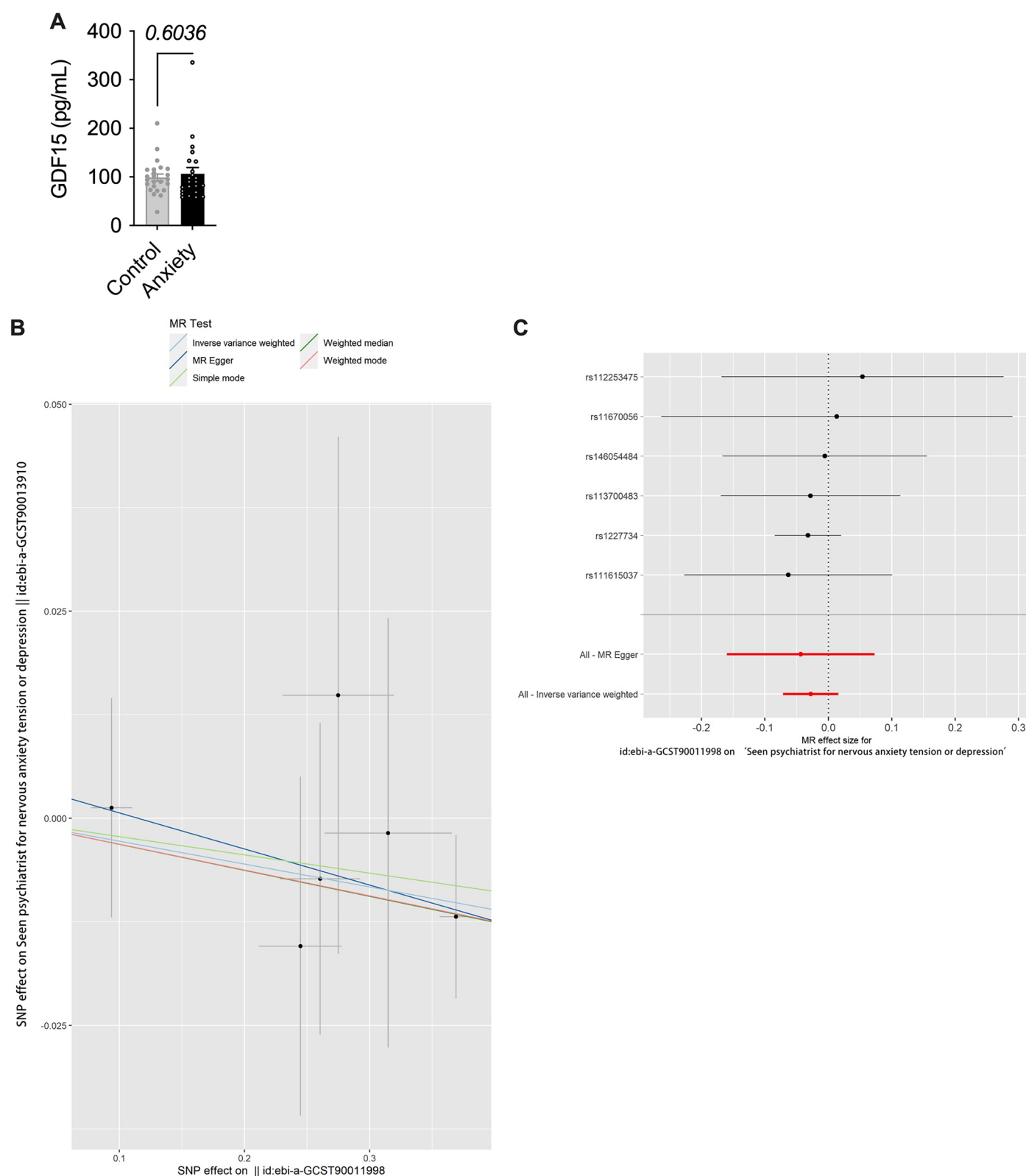
© The Author(s), under exclusive licence to Springer Nature Limited 2025

¹Centre for Metabolism, Obesity and Diabetes Research, McMaster University, Hamilton, Ontario, Canada. ²Division of Endocrinology and Metabolism, Department of Medicine, McMaster University, Hamilton, Ontario, Canada. ³Sunnybrook Research Institute, University of Toronto, Toronto, Ontario, Canada. ⁴Department of Health Science, Brock University, St. Catharines, Ontario, Canada. ⁵Department of Anesthesiology, Washington University in St. Louis, St. Louis, MO, USA. ⁶Department of Biochemistry and Biomedical Sciences, McMaster University, Hamilton, Ontario, Canada. ⁷Human Health and Nutritional Science, University of Guelph, Guelph, Ontario, Canada. ⁸Farncombe Family Digestive Health Research Institute, McMaster University, Hamilton, Ontario, Canada. ⁹School of Kinesiology, University of British Columbia, Vancouver, British Columbia, Canada. ¹⁰British Columbia Children's Hospital Research Institute, Vancouver, British Columbia, Canada. ¹¹Faculty of Land and Food Systems, University of British Columbia, Vancouver, British Columbia, Canada. ¹²Department of Kinesiology, Brock University, St. Catharines, Ontario, Canada. ¹³Department of Pediatrics, McMaster University, Hamilton, Ontario, Canada. ¹⁴Department of Medicine, Faculty of Medicine and Health Sciences, Université de Sherbrooke, Centre de recherche du Centre hospitalier universitaire de Sherbrooke, Sherbrooke, Quebec, Canada. ¹⁵David Braley Cardiac, Vascular and Stroke Research Institute, Hamilton, Ontario, Canada. ¹⁶Hamilton General Hospital, Hamilton Health Sciences, Hamilton, Ontario, Canada. ¹⁷Department of Surgery, McMaster University, Hamilton, Ontario, Canada. ✉e-mail: gstein@mcmaster.ca



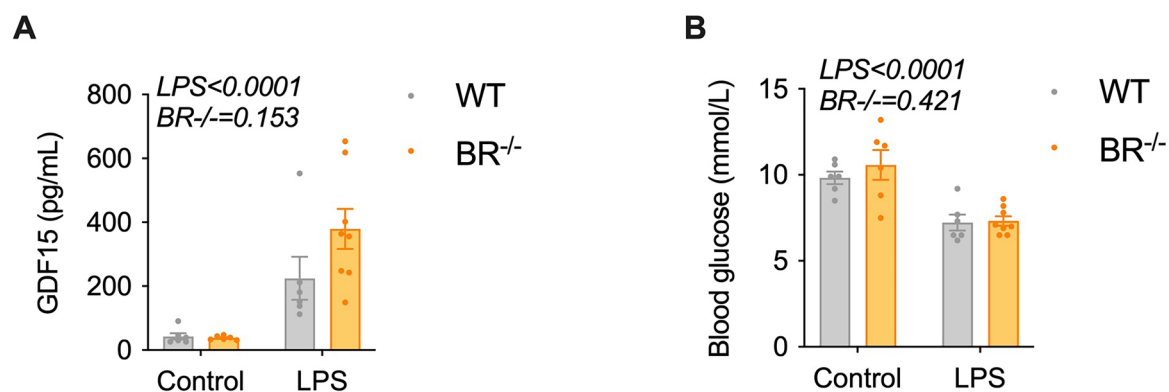
Extended Data Fig. 1 | Sex- and housing temperature-independent effects of exogenous epinephrine on GDF15. **a)** Pathway analysis from RNA-sequencing of gWAT following 1-hr epinephrine treatment. $n = 6$ per group. **b)** Heat map showing ligand-encoded genes from RNA-sequencing of gWAT following 1-hr epinephrine treatment. $n = 6$ per group. **c)** Circulating GDF15 from age-matched male (saline $n = 9$, epinephrine $n = 9$) and female mice (saline $n = 10$, epinephrine $n = 11$) following 1-hr epinephrine with fold-change relative to baseline levels (inset). Data presented as mean \pm s.e.m. with p-values calculated using 2-way

ANOVA with post-hoc test and Tukey's correction and unpaired two-tail t-test, respectively. **d)** Time-course of circulating GDF15 post-saline (RT $n = 5$, TN $n = 4$) or epinephrine (RT $n = 5$, TN $n = 5$) in mice housed at room temperature (RT - 22 °C) or thermoneutrality (TN - 29 °C) for 4 weeks. $n = 4$ -5/group. Data presented as mean \pm s.e.m. with p-values calculated using 2-way ANOVA at each time point. **e)** Serum epinephrine in control ($n = 9$ mice), 1-hr post IP epinephrine ($n = 7$), and 4-hr physical restraint ($n = 8$). Data presented as mean \pm s.e.m. with p-values calculated using 1-way ANOVA with post-hoc test and Tukey's correction.



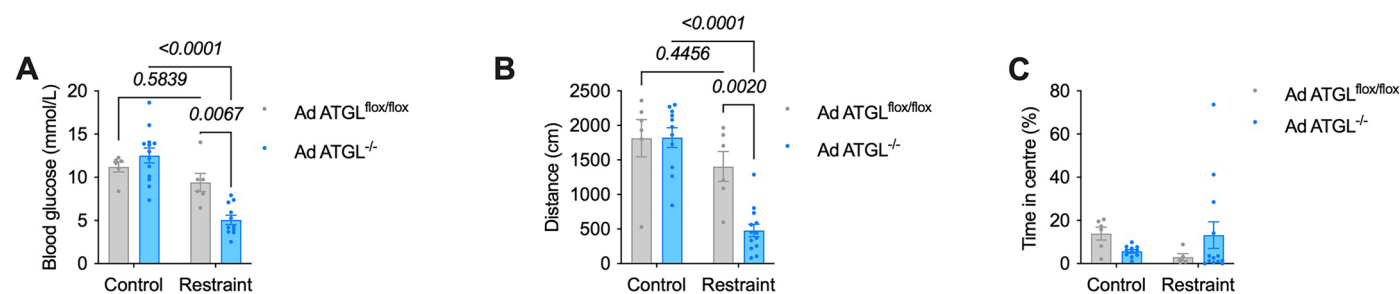
Extended Data Fig. 2 | Chronic psychological stress not associated with elevated circulating GDF15 levels in humans. a) Serum GDF15 levels in children with overweight and obesity with ($n = 23$) or without ($n = 24$) diagnosis of anxiety. Data presented as mean \pm s.e.m. with p-values calculated using unpaired two-tail t-test. **b)** Scatter plot of the SNP-effect on GDF15 and single nucleotide polymorphism (SNP)-effect on nervous anxiety tension or depression in humans by using two sample Mendelian Randomization (2SMR). Data presented as mean

\pm error bars indicate 95% CI, $n = 407,746$ participants in UK Biobank. MR analysis was performed by using Simple median method, MR weighted mode estimator, Weighted median method, MR Egger regression, Inverse variance weighted methods. **c)** Single SNP analysis of GDF15 on anxiety and depression in humans, Data presented as mean \pm error bars indicate 95% CI, $n = 407,746$ participants in UK Biobank.



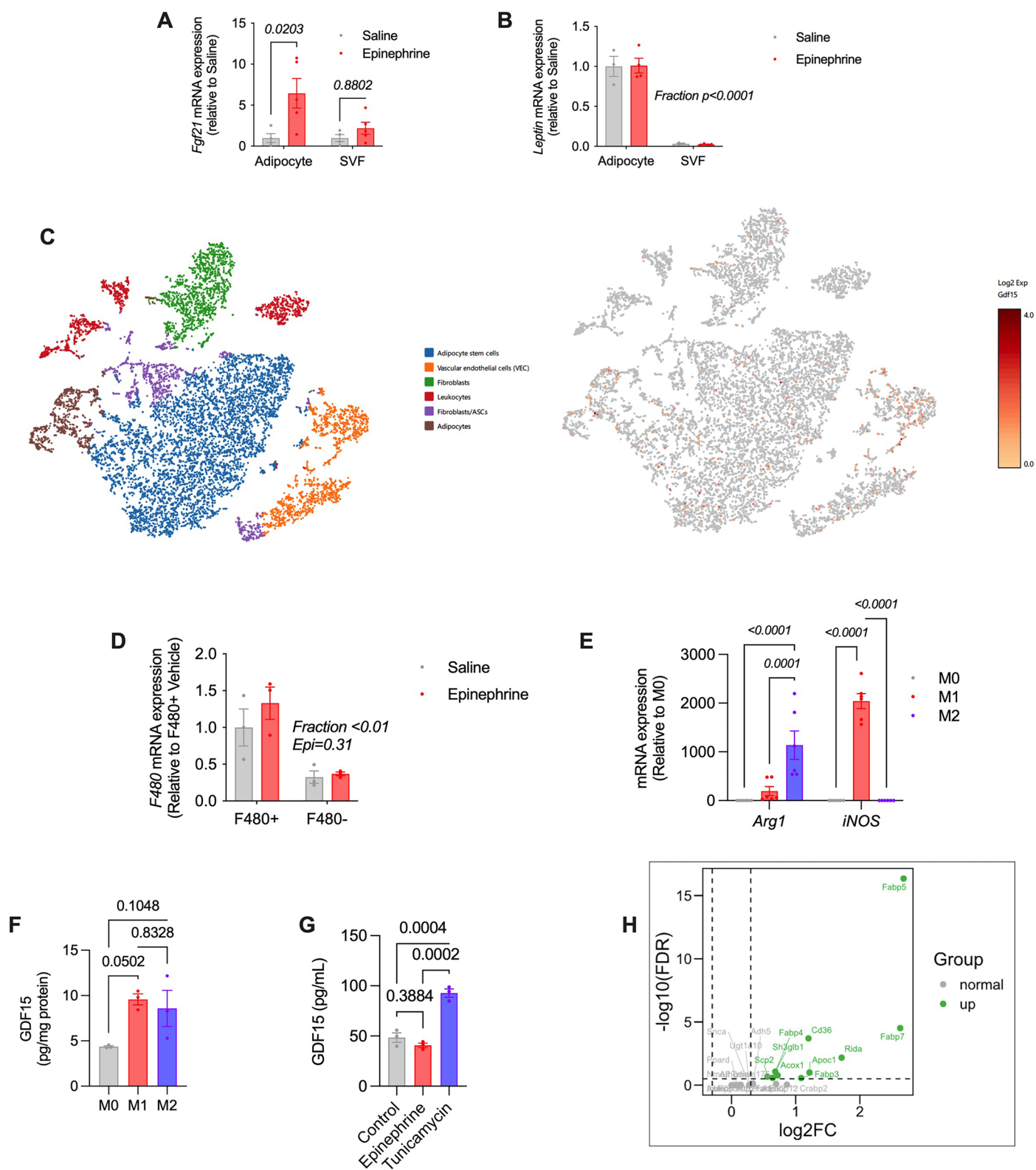
Extended Data Fig. 3 | Effects of LPS in beta receptor knockout mice. a) Serum GDF15 from WT and β -adrenergic receptor knockout (BR^{-/-}) mice following 2-hr LPS treatment (WT $n = 6$, BR^{-/-} $n = 6$) or control (WT $n = 6$, BR^{-/-} $n = 8$). Data presented as mean \pm s.e.m. with p-values calculated using 2-way ANOVA. **b)** Blood

glucose from WT and BR^{-/-} mice following 2-hr LPS treatment (WT $n = 6$, BR^{-/-} $n = 6$) or control (WT $n = 6$, BR^{-/-} $n = 8$). Data presented as mean \pm s.e.m. with p-values calculated using 2-way ANOVA.



Extended Data Fig. 4 | Restraint stress in AdATGL^{flox/flox} and AdATGL^{-/-} mice.
a) Blood glucose levels in AdATGL^{flox/flox} mice (control $n = 6$, restraint $n = 6$) and AdATGL^{-/-} (control $n = 13$, restraint $n = 11$). Data presented as mean \pm s.e.m. with p-values calculated using 2-way ANOVA with post-hoc test and Tukey's correction. **b)** Total distance for AdATGL^{flox/flox} mice (control $n = 6$, restraint $n = 6$) and AdATGL^{-/-} (control $n = 13$, restraint $n = 11$) during open-field test. Data

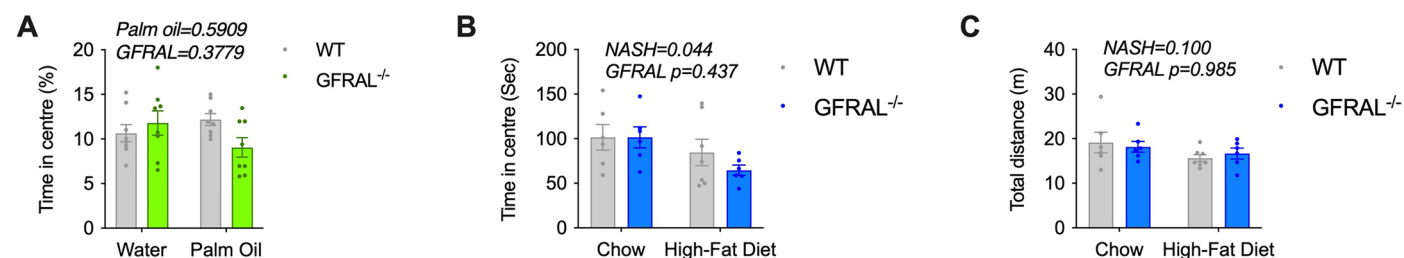
presented as mean \pm s.e.m. with p-values calculated using 2-way ANOVA with post-hoc test and Tukey's correction. **c)** Time in the centre for AdATGL^{flox/flox} mice (control $n = 6$, restraint $n = 6$) and AdATGL^{-/-} (control $n = 13$, restraint $n = 11$) during open-field test. Data presented as mean \pm s.e.m. with no statistical test performed.



Extended Data Fig. 5 | See next page for caption.

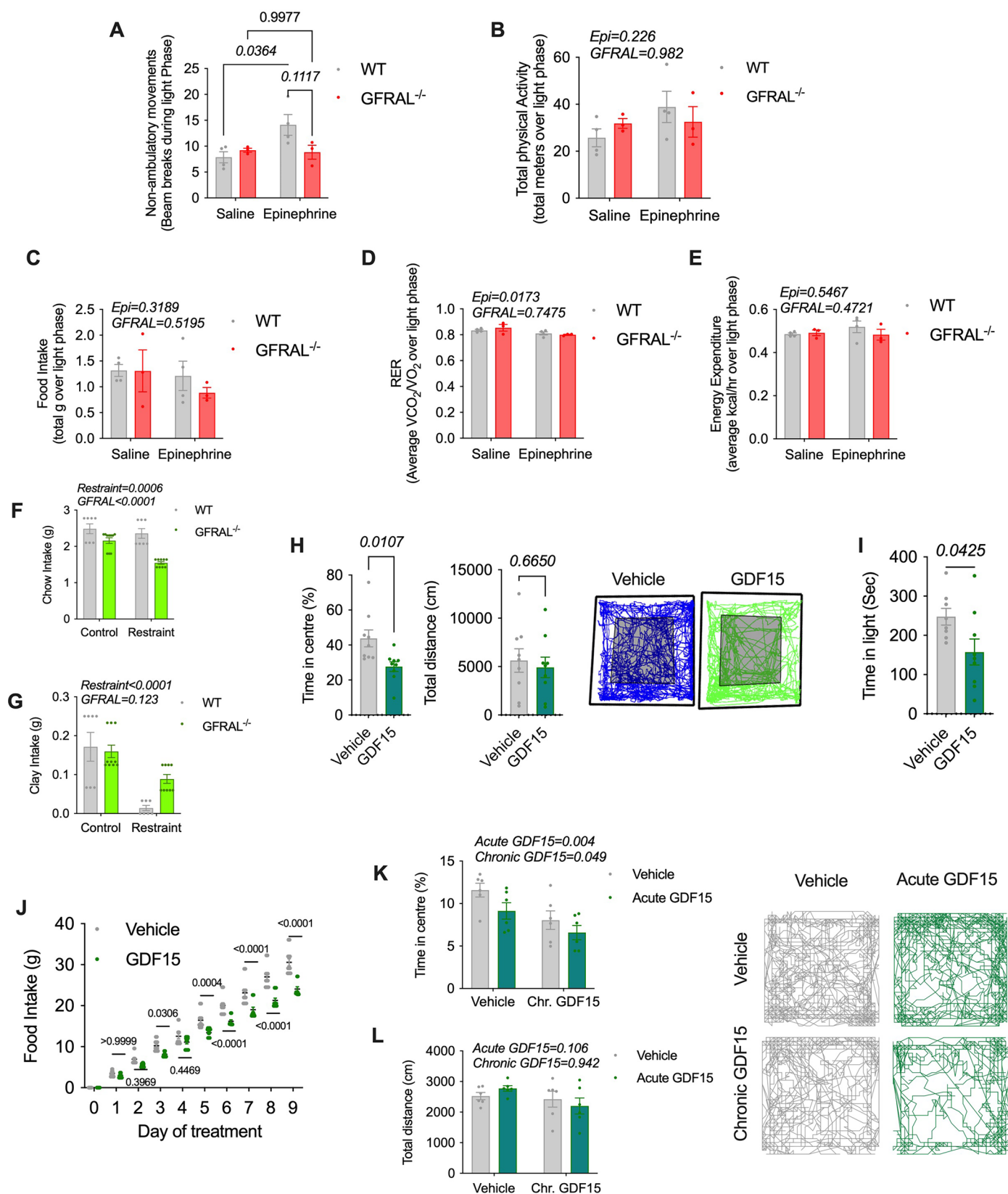
Extended Data Fig. 5 | Macrophages are the most likely source of GDF15 within adipose tissue. a) *Fgf21* expression in mouse adipocyte and SVF from gWAT post-saline ($n = 4$ per group) or epinephrine ($n = 5$ per group). Data presented as mean \pm s.e.m. with p-values calculated using 2-way ANOVA with post-hoc test and Tukey's correction. **b)** *Leptin* expression in mouse adipocyte and SVF from gWAT post-saline ($n = 3$ per group) or epinephrine ($n = 4$ per group). Data presented as mean \pm s.e.m. with p-values calculated using 2-way ANOVA. **c)** t-SNE plot of Lin-stromal vascular cells from gWAT of control mice and mice treated with CL for 3 days. Clustering identified 6 major cell types/states. Clusters are highlighted in different colors. The data set was queried for cells expressing *Gdf15*. Heatmap shows expression of *Gdf15* and other cell-identifying factors in the various identified cell populations. **d)** *F480/Adgre1* expression in mouse F480+ and F480- fractions of SVF from gWAT 1-hr post-epinephrine treatment (0.5 mg/kg). Data presented as mean \pm s.e.m. with $n = 3$ per group. p-values calculated using 2-way ANOVA. **e)** *Arg1* and *Nos2* expression in bone marrow-derived

macrophages (BMDMs) polarized to either M1-like or M2-like. $n = 6$ per group. Individual data points represent duplicates from 3 independent experiments. Data presented as mean \pm s.e.m. with p-values calculated using 1-way ANOVA with post-hoc test and Tukey's correction. **f)** GDF15 levels in media from BMDMs polarized to either M1-like or M2-like for 24-hrs. $n = 3$ per group. Individual data points represent triplicates from 3 independent experiments. Data presented as mean \pm s.e.m. with p-values calculated using 1-way ANOVA with post-hoc test and Tukey's correction. **g)** GDF15 levels in media from M2-like BMDMs treated with epinephrine (1 μ M) or tunicamycin (5 ng/mL) for 24-hrs. $n = 3$ per group. Individual data points represent triplicates from 3 independent experiments. Data presented as mean \pm s.e.m. with p-values calculated using 1-way ANOVA with post-hoc test and Tukey's correction. **h)** Volcano plot showing fatty acid transporters identified between M1- and M2-like macrophage populations from scRNA-seq data.



Extended Data Fig. 6 | Lipids and anxiety. a) Time in the centre during open-field test (% total) following 4-hr palm oil gavage (10 mL/kg) gavage in WT and *Gfral*^{-/-} mice. *n* = 8 per group. Data presented as mean ± s.e.m. with p-values calculated using 2-way ANOVA. **b)** Time in the centre during open-field test for chow (WT *n* = 6 mice, *Gfral*^{-/-} *n* = 6) or 4-week high-fat diet fed mice (WT *n* = 7 mice, *Gfral*^{-/-}

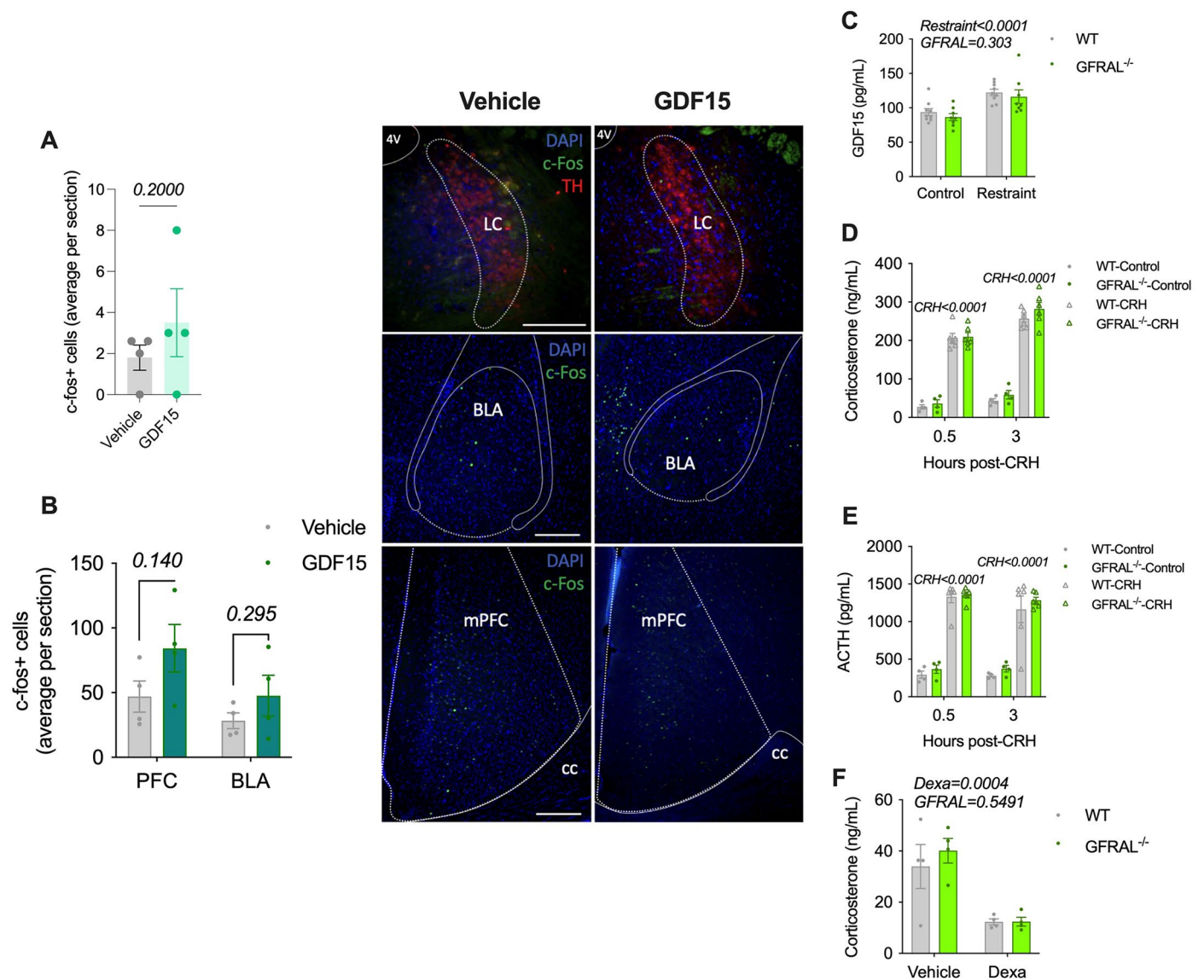
n = 6). Data presented as mean ± s.e.m. with p-values calculated using 2-way ANOVA. **c)** Total distance traveled during open-field test for chow (WT *n* = 6 mice, *Gfral*^{-/-} *n* = 6) or 4-week high-fat diet fed mice (WT *n* = 7 mice, *Gfral*^{-/-} *n* = 6). Data presented as mean ± s.e.m. with p-values calculated using 2-way ANOVA.



Extended Data Fig. 7 | See next page for caption.

Extended Data Fig. 7 | GDF15-GFRAL signalling is important for behavioural responses to epinephrine. **a)** Non-ambulatory movements, **b)** Total physical activity, **c)** Total food intake, **d)** respiratory exchange ratio (RER), **e)** Energy expenditure in WT (saline $n = 4$, epinephrine $n = 4$) and *Gfral*^{-/-} mice (saline $n = 4$, epinephrine $n = 4$). Data presented as mean \pm s.e.m. with p-values calculated using 2-way ANOVA with post-hoc test and Tukey's correction. **f)** Chow intake (18-hrs) following tube restraint in WT (control $n = 7$, restraint $n = 7$) and *Gfral*^{-/-} mice (control $n = 10$, restraint $n = 9$). Data presented as mean \pm s.e.m. with p-values calculated using 2-way ANOVA. **g)** Kaolin clay intake (18-hrs) following tube restraint in WT (control $n = 7$, restraint $n = 7$) and *Gfral*^{-/-} mice (control $n = 10$, restraint $n = 9$). Data presented as mean \pm s.e.m. with p-values calculated using 2-way ANOVA. **h)** Time in center and total distance during open-field test following GDF15 treatment with representative images showing movement of individual mice. $n = 9$ per group. Data presented as mean \pm s.e.m. with p-values

calculated using unpaired two-tail t-test. **i)** Time in light during light-dark box test following vehicle ($n = 8$) or GDF15 treatment ($n = 9$). Data presented as mean \pm s.e.m. with p-values calculated using unpaired two-tail t-test. **j)** Daily chow food intake throughout repeated GDF15 (5 nM/kg IP). $n = 12$ per group. Data presented as mean \pm s.e.m. with p-values calculated using 2-way ANOVA with post-hoc test and Tukey's correction. **k)** Time in the center during open-field test following GDF15 treatment (5 nM/kg IP) with representative images of movement of individual mice. $n = 6$ per group. Data presented as mean \pm s.e.m. with p-values calculated using 2-way ANOVA. Chr. GDF15: Chronic GDF15. **l)** Total distance traveled during open-field test following GDF15 treatment (5 nM/kg IP) with representative images showing representative movement of individual mice. $n = 6$ per group. Data presented as mean \pm s.e.m. with p-values calculated using 2-way ANOVA. Chr. GDF15: Chronic GDF15.



Extended Data Fig. 8 | Neither the locus coeruleus, nor its angiogenic downstream brain regions, are activated by GDF15. a Quantification of c-Fos positive cells in the locus coeruleus 90-min following GDF15 treatment (5 nm/kg IP), with representative pictures of the staining for TH and c-Fos. $n = 4$ per group. Data presented as mean \pm s.e.m. with p-values calculated using unpaired two-tail t-test. Scale bar = 200 μ m. 4V: 4th ventricle, LC: locus coeruleus, TH: tyrosine hydroxylase. **b** Quantification of c-Fos positive cells in the PFC and BLA 90-min following GDF15 treatment (5 nm/kg IP), with representative pictures of the staining. $n = 4$ per group. Data presented as mean \pm s.e.m. with p-values calculated using unpaired two-tail t-test. Scale bar = 200 μ m. BLA: basolateral amygdala, cc: corpus callosum, mPFC: medial prefrontal cortex.

c Serum GDF15 in WT (control $n = 9$, restraint $n = 9$) and Gfral^{-/-} mice (control $n = 8$, restraint $n = 8$). Data presented as mean \pm s.e.m. with p-values calculated using 2-way ANOVA with Tukey's post-hoc correction. **d** Serum corticosterone in WT (control $n = 4$, CRH $n = 6$) and Gfral^{-/-} mice (control $n = 4$, CRH $n = 6$). Data presented as mean \pm s.e.m. with p-values calculated using 2-way ANOVA at each timepoint. **e** Serum adrenocorticotropic hormone (ACTH) in WT (control $n = 4$, CRH $n = 6$) and Gfral^{-/-} mice (control $n = 4$, CRH $n = 6$). Data presented as mean \pm s.e.m. with p-values calculated using 2-way ANOVA at each timepoint. **f** Serum corticosterone 6-hr post treatment with dexamethasone (Dexa, 100 μ g/kg IP). $n = 4$ per group. Data presented as mean \pm s.e.m. with p-values calculated using 2-way ANOVA.

Reporting Summary

Nature Portfolio wishes to improve the reproducibility of the work that we publish. This form provides structure for consistency and transparency in reporting. For further information on Nature Portfolio policies, see our [Editorial Policies](#) and the [Editorial Policy Checklist](#).

Statistics

For all statistical analyses, confirm that the following items are present in the figure legend, table legend, main text, or Methods section.

- | | |
|-------------------------------------|--|
| n/a | Confirmed |
| <input type="checkbox"/> | <input checked="" type="checkbox"/> The exact sample size (<i>n</i>) for each experimental group/condition, given as a discrete number and unit of measurement |
| <input type="checkbox"/> | <input checked="" type="checkbox"/> A statement on whether measurements were taken from distinct samples or whether the same sample was measured repeatedly |
| <input type="checkbox"/> | <input checked="" type="checkbox"/> The statistical test(s) used AND whether they are one- or two-sided
<i>Only common tests should be described solely by name; describe more complex techniques in the Methods section.</i> |
| <input type="checkbox"/> | <input checked="" type="checkbox"/> A description of all covariates tested |
| <input type="checkbox"/> | <input checked="" type="checkbox"/> A description of any assumptions or corrections, such as tests of normality and adjustment for multiple comparisons |
| <input type="checkbox"/> | <input checked="" type="checkbox"/> A full description of the statistical parameters including central tendency (e.g. means) or other basic estimates (e.g. regression coefficient) AND variation (e.g. standard deviation) or associated estimates of uncertainty (e.g. confidence intervals) |
| <input type="checkbox"/> | <input checked="" type="checkbox"/> For null hypothesis testing, the test statistic (e.g. <i>F</i> , <i>t</i> , <i>r</i>) with confidence intervals, effect sizes, degrees of freedom and <i>P</i> value noted
<i>Give P values as exact values whenever suitable.</i> |
| <input checked="" type="checkbox"/> | <input type="checkbox"/> For Bayesian analysis, information on the choice of priors and Markov chain Monte Carlo settings |
| <input checked="" type="checkbox"/> | <input type="checkbox"/> For hierarchical and complex designs, identification of the appropriate level for tests and full reporting of outcomes |
| <input type="checkbox"/> | <input checked="" type="checkbox"/> Estimates of effect sizes (e.g. Cohen's <i>d</i> , Pearson's <i>r</i>), indicating how they were calculated |

Our web collection on [statistics for biologists](#) contains articles on many of the points above.

Software and code

Policy information about [availability of computer code](#)

Data collection	immunofluorescence images were acquired using Zeiss Axio Scan 7. Protein bands for Western blotting were visualized with the MBI Fusion FX7 system.
Data analysis	For Two-sample Mendelian Randomization analysis, we used TwoSampleMR R package (v0.5.6) from https://mrcieu.github.io/twosampleMR/ . For RNA-Seq analyses, we used MultiQC (v1.12), trim galore (v0.6.5-1), Salmon (v1.10.1), DESeq2 (v1.38.3), GOstats (v2.64.0), KEGG.db (v3.2.3), cnetplots for R. RNA Sequencing visualizations were performed in R. The single cell RNA-Seq data used for the analyses described in this article were obtained from the NCBI Sequence Read Archive under reference number SRP14547526. The Cell Ranger was used to perform sample qualifying, alignment, filtering, counting, and aggregation using the Linux system or the R and RStudio software. Clustering and gene expression were visualized with 10X Genomics Loupe Browser (v.6.5.0). Statistical analyses were performed in Prism (version 10), R (Version 4.2.3), or RStudio software (Version 1.3.1056). MATLAB (v2022b) were used for analyses of open-field tests. Western Blot images were quantified using Image J software

For manuscripts utilizing custom algorithms or software that are central to the research but not yet described in published literature, software must be made available to editors and reviewers. We strongly encourage code deposition in a community repository (e.g. GitHub). See the Nature Portfolio [guidelines for submitting code & software](#) for further information.

Data

Policy information about [availability of data](#)

All manuscripts must include a [data availability statement](#). This statement should provide the following information, where applicable:

- Accession codes, unique identifiers, or web links for publicly available datasets
- A description of any restrictions on data availability
- For clinical datasets or third party data, please ensure that the statement adheres to our [policy](#)

FASTQ files from these scRNA-seq libraries are available at the Pique-Regi lab webpage (<http://piquelab.grid.wayne.edu/>), as well as the Sequence Read Archive (SRA; <https://www.ncbi.nlm.nih.gov/sra/>) (SRA: SRP145475). Scripts for data processing are available through GitHub (<https://github.com/RBBurl1227>). The data that support the findings of this study are available from the corresponding author upon request

Research involving human participants, their data, or biological material

Policy information about studies with [human participants or human data](#). See also policy information about [sex, gender \(identity/presentation\), and sexual orientation](#) and [race, ethnicity and racism](#).

Reporting on sex and gender

Unless otherwise stated only male mice were used in this study. For mouse experiments where male and female mice were compared, age-matched litter mates were used. Biological sex was considered, and reported, where possible in human analyses.

Reporting on race, ethnicity, or other socially relevant groupings

Not Applicable

Population characteristics

Children with obesity who were enrolled in the Canadian Pediatric Weight management Registry (CANPWR) at the McMaster site were included in this study. Study participants with an available fasting blood sample at their initial visit and a clinical diagnosis of anxiety but without use of antipsychotic or antidepressant medications (n=23) were compared to those without any diagnosis of anxiety and also free from use of medications (n=24). Participants were matched for age (12.50+/-2.97 and 12.44+/-2.86 years of age), sex (12/11 and 12/12 male/female), body weight (87+/-31.88 and 88+/-35.32 kg), and body mass index (33.18+/-6.41 and 34.08+/-8.07) between control and participants with anxiety, respectively.

Recruitment

Not Applicable

Ethics oversight

Animal studies were carried out at McMaster University (210104), University of Toronto (21-467 and 24-0362H), or Washington University in St. Louis (20-0139). All animals used in the study were housed and cared for in accordance with the Guidelines for Animal Use at McMaster University and were approved by the McMaster University Animal Ethics Research Board or their respective facilities Ethics Boards.

Note that full information on the approval of the study protocol must also be provided in the manuscript.

Field-specific reporting

Please select the one below that is the best fit for your research. If you are not sure, read the appropriate sections before making your selection.

☒ Life sciences ☐ Behavioural & social sciences ☐ Ecological, evolutionary & environmental sciences

For a reference copy of the document with all sections, see nature.com/documents/nr-reporting-summary-flat.pdf

Life sciences study design

All studies must disclose on these points even when the disclosure is negative.

Sample size

No statistical test was used to determine sample size but sample size for all animal studies were based on well-established protocols previously performed in authors' labs (Wang et al., Nature, 2023; Day et al. Nature Metabolism, 2019; McCall et al. 2015, Nueon; McCall et al. 2017, eLife; Blondin et al. 2022, Cell Metabolism) and provide adequate power to detect the substantial effect while ensuring no more animals that necessary were used. In vitro sample size were based on previous experience (Townsend et al. 2021, FASEB; Day et al. 2019, Nature Metabolism). Sample size was also informed by animal availability, homogeneity, and consistency of characteristics of selected animals.

Data exclusions

Data were excluded only if statistically confirmed as outlier: 1 sample from BAT in Figure 1G; 2 mice Figure 1H; 1 mouse from Figure 3B, 1 mouse from Extended Data Figure 1A. One participant was excluded from pediatric analysis as it was inappropriately included by human error. Exclusions did not affect interpretation of results.

Replication

Nearly all experiments were completed across at least 2 independent cohorts. All cell-based experiments are from 3 independent experiments. All attempts at replication were successful.

Randomization	Prior to experimentation animals were randomly assigned to groups. For human participants the recruitment, collection, and sample selection was completed by a blinded researcher. Participants were matched by researcher prior to analysis.
Blinding	Investigators were blinded to experimental groups during tissue collection. During behavioural tests blinding was not possible during experiment as drug administration was required by subsequent behavioural analyses of tests was performed by blinded researcher.

Reporting for specific materials, systems and methods

We require information from authors about some types of materials, experimental systems and methods used in many studies. Here, indicate whether each material, system or method listed is relevant to your study. If you are not sure if a list item applies to your research, read the appropriate section before selecting a response.

Materials & experimental systems

n/a	Involved in the study
<input type="checkbox"/>	<input checked="" type="checkbox"/> Antibodies
<input type="checkbox"/>	<input checked="" type="checkbox"/> Eukaryotic cell lines
<input checked="" type="checkbox"/>	<input type="checkbox"/> Palaeontology and archaeology
<input type="checkbox"/>	<input checked="" type="checkbox"/> Animals and other organisms
<input type="checkbox"/>	<input checked="" type="checkbox"/> Clinical data
<input checked="" type="checkbox"/>	<input type="checkbox"/> Dual use research of concern
<input checked="" type="checkbox"/>	<input type="checkbox"/> Plants

Methods

n/a	Involved in the study
<input checked="" type="checkbox"/>	<input type="checkbox"/> ChIP-seq
<input checked="" type="checkbox"/>	<input type="checkbox"/> Flow cytometry
<input checked="" type="checkbox"/>	<input type="checkbox"/> MRI-based neuroimaging

Antibodies

Antibodies used	Phosphorylated PKA substrates (1:1000 dilution, Cell Signalling Technology, Catalogue #9624, lot 10) beta-tubulin (1:1000 dilution, Abcam, catalogue number #ab4074) c-Fos (1:1000 dilution, Cell Signaling Technology Cat# 2250s) TH (1:1000dilution, Aves Lab, Cat#TYH)
Validation	<p>All antibodies were used in accordance to the manufacturer guidelines.</p> <p>Western blotting remains one of the most common scientific methods for monitoring protein expression in cells or tissue. The accuracy of western blot results relies heavily of the quality of the primary antibody employed in the immunoblotting. Cell Signaling Technology (CST) provides the highest quality primary and secondary antibodies available for western blotting. CST™ antibodies are produced in-house and validated extensively according to a rigorous protocol.</p> <p>Validation Steps Include Examination of several cell lines and/or tissues of known expression levels allows accurate determination of species cross-reactivity and verifies specificity. Treatment of cell lines with growth factors, chemical activators or inhibitors, which induce or inhibit target expression, verifies specificity. Phosphatase treatment confirms phospho-specificity. The use of siRNA transfection or knockout cell lines verifies target specificity. Side-by-side comparison of lots to ensures lot-to-lot consistency. Optimal dilutions and buffers are predetermined, positive and negative cell extracts are specified, and detailed protocols are already optimized, saving valuable time and reagents.</p>

Eukaryotic cell lines

Policy information about [cell lines and Sex and Gender in Research](#)

Cell line source(s)	Bone marrow-derived macrophages were isolated from mice and confirmed by gene expression signatures, as done previously in our lab (Day et al. 2023, Cell Reports; Morrow et al. 2022, Cell Metabolism) White adipocytes were generated and differentiated as previously described by our lab (Mottillo et al. 2016, Cell Metabolism 10.1016/j.cmet.2016.06.006)
Authentication	Cell lines were authenticated by appropriate gene signatures and physiological responses herein.
Mycoplasma contamination	Not Applicable
Commonly misidentified lines (See ICLAC register)	Not Applicable

Animals and other research organisms

Policy information about [studies involving animals](#); [ARRIVE guidelines](#) recommended for reporting animal research, and [Sex and Gender in Research](#)

Laboratory animals	Germline GFRAL knockout mice (Gfral ^{-/-}), b1, b2, b3-adrenergic receptors triple knockout mice, Atgl/Pnpla2-floxed and Atgl/Pnpla2 knockout mice used in this study were on a C57bl/6j background, all males unless otherwise stated, and between the ages of 16-24 weeks for experiments. Mice were housed in temperature controlled either ambient (~22C at 40-60% relative humidity) or thermoneutral conditions (~29C).
Wild animals	No wild animals were used.
Reporting on sex	Unless otherwise stated only male mice were used in this study.
Field-collected samples	No field-collected samples were used.
Ethics oversight	Guidelines for Animal Use at McMaster University and were approved by the McMaster University Animal Ethics Research Board (AUP 210104) or their respective facilities Ethics Boards

Note that full information on the approval of the study protocol must also be provided in the manuscript.

Clinical data

Policy information about [clinical studies](#)

All manuscripts should comply with the ICMJE [guidelines for publication of clinical research](#) and a completed [CONSORT checklist](#) must be included with all submissions.

Clinical trial registration	Clinicaltrials.gov identifier NCT02811289.
Study protocol	Full protocols for experiments have been previously published. Pediatric samples : Morrison et al. 2014, BMC Pediatrics, 10.1186/1471-2431-14-161
Data collection	Please see previous publications for detailed descriptions of data collection and outcomes.
Outcomes	Please see previous publications for detailed descriptions of data collection and outcomes.

Plants

Seed stocks	Not Applicable
Novel plant genotypes	Not Applicable
Authentication	Not Applicable